

**BROADBAND AND HIGH FREQUENCY
PIEZOELECTRIC ENERGY HARVESTING SYSTEM
WITH CURVED PANELS FOR PASSIVE VIBRATION
ISOLATOR**

**PASİF TİTREŞİM İZOLATÖRÜ İÇİN KAVISLİ PANELLİ
GENİŞ BANT VE YÜKSEK FREKANSLI
PIEZOELEKTRİK ENERJİ HASAT SİSTEMİ**

OSMAN KIZILTAŞ

ASSOC. PROF. DR. BİLSAY SÜMER

Supervisor

Submitted to

Graduate School of Science and Engineering of Hacettepe University

as a Partial Fulfillment to the Requirements

for the Award of the Degree of Master of Science

in Mechanical Engineering

2023

ABSTRACT

BROADBAND AND HIGH FREQUENCY PIEZOELECTRIC ENERGY HARVESTING SYSTEM WITH CURVED PANELS FOR PASSIVE VIBRATION ISOLATOR

Osman KIZILTAŞ

Master of Science Degree, Department of Mechanical Engineering

Supervisor: Assoc. Prof. Dr. Bilsay SÜMER

Jan 2023, 74 Pages

In military aircrafts, random vibration occurs with high amplitude in broad frequency spectrum. High vibration profiles, which affecting electronic units, can cause fatigue over time and damage mechanics and electronic cards. Therefore, electronic units are integrated into aerial platforms via isolators to dampen vibration. The isolators significantly dampen the vibration exposure and significantly increase the life of the electronic units. Although they are mounted with isolators, it is of great importance to carry out instant health monitoring in order to prevent loosening and mechanical deformations that may cause vital problems.

The energy needs of all electronic devices used in our daily lives are provided through various sources. Micro-electromechanical systems used in health monitoring and data transfer need their own energy source because they are used in hard-to-reach areas. For this reason, energy production methods from alternative sources are being investigated. Piezoelectric materials, which have a high energy production capacity in narrow spaces and can produce energy in a wide vibration frequency band without the need for another electrical source, are one step ahead for energy harvesting.

Piezoelectric materials generate voltage through stresses caused by vibration on the surface to which they are attached. The voltage occurs harmonically at the vibration

frequency, positively and negatively charged. When the generated voltage is connected to the circuit, it creates alternating current. After the energy is regulated, the battery/capacitor can charge and power electronic devices. As a result, systems can operate without the need for an additional energy source as long as there is vibration.

In this thesis, energy harvesting from the piezoelectric material placed on the curved panels which are mounted on the isolators of the electronic unit subjected to military helicopter vibration profile. Curved panels on which piezoelectric patches are attached are mounted between the vibration source and the mass. Vibration acting on the isolator affected the curved panel with a higher profile than the vibration profile applied with phase difference and amplification. With the help of the natural frequencies of the curved panel, the piezoelectric materials were exposed to higher vibrations and produced high energy in a wider frequency band. Energy was produced by vibration, which is a completely undesirable energy encountered greatly on aerial platforms.

Dummy mass was used as electronic unit and isolators was selected in line with the determined mass. In the selection of mass and isolators, care has been taken to ensure that the system is the only natural frequency in the frequency band of interest. Measurements were made by giving white noise to the system and its behavior was examined and verifications were carried out.

Piezoelectric materials were adhered to the curved panel as 3 different patches. Curved panels and piezoelectric materials produced in the specified dimensions were driven by harmonic vibration and energy was produced. A finite element model of the system was created with the same dimensions with the help of Space Claim. The model was verified by performing finite element analysis using by Ansys. In the analysis study, the width, thickness and length of the piezoelectric patches were changed and the relative acceleration data measured in the isolator verification study was applied and sensitivity analysis was made.

Keywords: Broadband Energy Harvesting, Vibration Isolation, Curved Panel Energy Harvesting, Piezoelectric Analysis

ÖZET

PASİF TİTREŞİM İZOLATÖRÜ İÇİN KAVİSLİ PANELLİ GENİŞ BANT VE YÜKSEK FREKANSLI PİEZOELEKTRİK ENERJİ HASAT SİSTEMİ

OSMAN KIZILTAŞ

Yüksek Lisans, Makine Mühendisliği Bölümü

Tez Danışmanı: Doç. Dr. Bilsay SÜMER

Ocak 2023, 74 Sayfa

Askeri uçaklarda yüksek genlikte ve geniş frekans bandında titreşim meydana gelmektedir. Elektronik birimlere etki eden yüksek titreşim profilleri zamanla yorulmalara neden olarak mekanik ve elektronik kartlara zarar verebilmektedir. Bu nedenle elektronik birimler titreşimi sönmölemek için izolatörler aracılığıyla hava platformlarına entegre edilmektedir. İzolatörler, maruz kalınan titreşimi büyük oranda sönmömlerken birimlerin ömrünü kayda değer oranda artırmaktadır. İzolatörlerle monte edilmelerine rağmen zamanla meydana gelebilecek gevşeme ve mekanik deformasyonların hayati sorunlara neden olmasının önüne geçilebilmesi için anlık sağlık takibinin yapılması büyük önem taşımaktadır.

Gündelik hayatımızda kullanılan tüm elektronik cihazlarda enerji ihtiyaçları çeşitli kaynaklar aracılığıyla sağlanmaktadır. Sağlık takibi ve veri aktarımında kullanılan mikro-elektromekanik sistemler ise ulaşılması zor alanlarda kullanılması sebebiyle kendi enerji kaynağına ihtiyaç duymaktadır. Bu nedenle alternatif kaynaklardan enerji üretim yöntemleri araştırılmaktadır. Dar alanlarda yüksek enerji üretim kapasitesine sahip, başka elektrik kaynağına ihtiyaç duymadan geniş titreşim frekans bandında enerji üretimi gerçekleştirebilen piezoelektrik malzemeler enerji hasatlama için bir adım öne çıkmaktadır.

Piezoelektrik malzemeler yapıştırıldığı yüzeyde titreşim kaynaklı oluşan gerilmeler aracılığıyla voltaj üretmektedir. Voltaj, pozitif ve negatif yüklü şekilde, titreşim

frekansında, harmonik olarak meydana gelmektedir. Üretilen voltaj devreye bağlandığında alternatif akım oluşturmaktadır. Enerji, regüle edilerek batarya/kapasitör şarj edebilmekte ve elektronik cihazlara güç vermektedir. Sonuç olarak titreşim olduğu sürece ek bir enerji kaynağına ihtiyaç duyulmadan sistemler çalışabilmektedir.

Bu tez çalışmasında, askeri uçaklara izolatörlerle bağlanan elektronik birimlerin izolatörlerine yerleştirilen kavisli panele yapıştırılan piezoelektrik malzemedeki enerji hasatlanması simüle edilmiştir. Titreşim kaynağı ile kütle arasında, üzerine piezoelektrik yamalar yapıştırılan kavisli paneller monte edilmiştir. İzolatöre etki eden titreşim, faz farkı ve amplifikasyon ile uygulanan titreşim profilinden daha yüksek profil ile kavisli panele etki etmiştir. Kavisli panelin doğal frekansları sayesinde piezoelektrik malzemeler daha yüksek titreşimlere maruz kalmış ve daha geniş frekans bandında yüksek enerji üretimi gerçekleştirmiştir. Hava platformlarda yoğun miktarda karşılaşılan tamamen istenmeyen bir enerji olan titreşimden faydalanılarak enerji üretimi yapılmıştır.

Elektronik birim olarak kukla kütle kullanılmıştır ve belirlenen kütle doğrultusunda izolatör seçimi yapılmıştır. Kütle ve izolatör seçiminde ilgilenilen frekans bandında sistemin tek doğal frekansı olmasına özen gösterilmiştir. Sisteme beyaz gürültü verilerek ölçümler yapılmıştır ve davranışları incelenmiş ve doğrulamalar gerçekleştirilmiştir.

Piezoelektrik malzemeler, kavisli panel üzerine 3 farklı yama olarak yapıştırılmıştır. Belirlenen boyutlarda üretilen kavisli panel ve piezoelektrik malzemeler harmonik titreşim ile tahrik edilerek enerji üretimi gerçekleştirilmiştir. Space Claim kullanılarak aynı boyutlarda sistemin sonlu elemanlar modeli oluşturulmuştur. Ansys yardımıyla sonlu elemanlar analizi yapılarak model doğrulanmıştır. Analiz çalışmasında piezoelektrik yamaların genişlikleri, kalınlıkları ve uzunlukları değiştirilerek izolatör doğrulama çalışmasında ölçülen bağıl ivme verileri uygulanarak optimizasyon yapılmıştır. Yapılan her boyut değişikliği için her bir yamanın enerji çıktısı ve enerji verimi değerlendirilmiş ve karşılaştırmalar yapılmıştır.

Anahtar Kelimeler: Piezoelektrik Enerji Hasatlama, Kavisli Panel, Geniş Frekans Bandında Enerji Hasatlama, Titreşim Sönümlenme

ACKNOWLEDGEMENTS

I would like to express my appreciation to my supervisor, Assoc. Prof. Dr. Bilsay SÜMER for his leading guidance and contributions throughout this thesis.

I want to thank with my deepest gratitude to my mentor Dr. Güvenç Canbaloglu for his leading guidance, helpful critics and technical supports.

I would like express my sincere gratitude to my colleague, Onur Okcu for making it easier for his technical support and recommendations at every step of this study.

I also would like to thank my colleagues, Ahmet Özdemir, Bora Deveci and Öner Murat Akbaba for their moral support and help during experiments.

I want to thank my managers and ASELSAN Inc. for giving me the opportunity to use the testing laboratories during my thesis.

Finally, I would like to express my huge appreciation to my dear wife and family for their unwavering moral support and trust throughout this study as in every stage of my life.

TABLE OF CONTENTS

ABSTRACT	i
ÖZET	iii
ACKNOWLEDGEMENTS	v
TABLE OF CONTENTS	vi
LIST OF FIGURES	viii
LIST OF TABLES	x
LIST OF SYMBOLS AND ABBREVIATIONS.....	xi
1. INTRODUCTION.....	1
1.1. Motivation	1
1.2. Scope of the Thesis	2
1.3. Thesis Outline	2
2. LITERATURE SURVEY	4
2.1. Vibration Isolation.....	4
2.2. Energy Harvesting.....	6
2.3. Vibration Isolation and Energy Harvesting.....	11
3. THEORY.....	12
3.1. Vibration Isolation.....	12
3.2. Energy Harvesting.....	14
4. VIBRATION ISOLATOR	16
4.1. Modal Test.....	17
4.1.1. Isolator Selection.....	17
4.1.2. Vibration Table Design	17
4.1.3. Dummy Mass Design	18
4.2. Test Setup.....	19
4.3. Experiment	22
4.4. Results	24
5. CURVED PANEL.....	31

5.1.	Curved Panel Experiment	31
5.1.1.	Curved Panel Specification.....	32
5.1.2.	Piezoelectric Patch Specification.....	32
5.2.	Experiment Setup.....	34
5.3.	Experiment Results	35
5.4.	Macro Fiber Composite (MFC) Experiment	38
6.	VERIFICATION OF FE MODEL	40
6.1.	Boundary Conditions	40
6.2.	Mesh Sensitivity Analysis	42
6.3.	Verification Analysis	43
7.	ENERGY HARVESTING SENSITIVITY ANALYSES	47
7.1.	Angle Sensitivity Analysis.....	49
7.2.	Width Sensitivity Analysis	53
7.3.	Thickness Sensitivity Analysis	56
7.4.	Selected Patches Verification	58
8.	CASE STUDIES	62
8.1.	Helicopter Vibration Profile	62
8.2.	Gun Fire Vibration Profile.....	64
8.3.	MFC	65
8.4.	CP Mode Sensitivity Analysis	67
9.	DISCUSSIONS AND CONCLUSION	69
	REFERENCES	72

LIST OF FIGURES

Figure 2.1 Conventional Vibration Isolation.....	5
Figure 2.2 Active Vibration Isolation [4].....	5
Figure 2.3 Vibration Isolators:	6
Figure 2.4 Mechanical Vibration Based Energy Harvesting Systems [12].....	7
Figure 2.5 Electromagnetic Energy Harvester [14]	7
Figure 2.6 Electrostatic Energy Harvester [16].....	8
Figure 2.7 Direct Piezoelectric Effect [19]	8
Figure 2.8 Reverse Piezoelectric Effect [19]	9
Figure 2.9 Working Frequency Range Change [23]	10
Figure 2.10 Curved Panel Energy Harvesting System [27]	11
Figure 2.11 Vibration Isolation and Energy Harvesting (VIEH) System Sample [31]...	12
Figure 3.1 SDOF Damped Base Excitation	12
Figure 3.2 SDOF Base Excited System: a) Transmissibility, b) Phase Angle Graphs ...	14
Figure 3.3 Piezoelectric Material Axes and Polarization Direction.....	15
Figure 4.1 1 st mode of Dummy Mass	19
Figure 4.2 A sample picture for the RI test setup.....	20
Figure 4.3 Imaginary Transmissibility of Left-Right Accelerometers.....	21
Figure 4.4 Real Transmissibility of Left-Right Accelerometers.....	21
Figure 4.5 White Noise 0.008 g ² /Hz	22
Figure 4.6 Input PSD.....	24
Figure 4.7 Imaginary Transmissibility for WRI.....	25
Figure 4.8 Real Transmissibility for WRI.....	25
Figure 4.9 Magnitude of Transmissibility for WRI	26
Figure 4.10 Magnitude of Transmissibility for EI	26
Figure 4.11 Output PSD of Each Axis	27
Figure 4.12 Natural Frequency for Each Input PSD of WRI.....	27
Figure 4.13 Damping Ratio for Each Input PSD of WRI	28
Figure 4.14 Output (Response) PSD of WRI.....	29
Figure 4.15 Relative Acceleration of WRI.....	30
Figure 5.1 First Two Modes of FE Model	33
Figure 5.2 Sample Piezoelectric Patch Pictures	33
Figure 5.3 A Sample Picture Showing the Shaker, Fixture & Connection Interface.....	34
Figure 5.4 Excitation Signal of the Mechanical Shaker.....	35

Figure 5.5 Acceleration-Time Data of PVDF Patches	36
Figure 5.6 Voltage-Time Data of PVDF Patches	36
Figure 5.7 Voltage-Frequency Data of PVDF Patches.....	37
Figure 5.8 Applied Acceleration of PVDF Patches	38
Figure 5.9 Voltage-Time Data of MFCs.....	39
Figure 5.10 Average Acceleration-Frequency Data of MFC	39
Figure 5.11 Voltage-Frequency Data of MFCs	40
Figure 6.1 FE Model Boundary Conditions.....	41
Figure 6.2 Mode Shapes of FE Model: 1 st mode (a), 2 nd mode (b), 3 rd mode (c).....	44
Figure 6.3 FEM Analysis Result vs. Test Result.....	45
Figure 6.4 Comparison of Applied Accelerations	47
Figure 7.1 Mode Shapes of Isolated FE Model:	48
Figure 7.2 Piezoelectric Patch Covered Angle Sensitivity Graph	50
Figure 7.3 Piezoelectric Patch Covered Angle Voltage Trend.....	51
Figure 7.4 Piezoelectric Patch Covered Angle VRMS Density Trend.....	52
Figure 7.5 Piezoelectric Patch Width Sensitivity Analysis Graph	54
Figure 7.6 Piezoelectric Patch Width Voltage RMS Trend.....	55
Figure 7.7 Piezoelectric Patch Width Voltage RMS Density Trend	56
Figure 7.8 Piezoelectric Patch Thickness Sensitivity Analysis Graph	57
Figure 7.9 Final Experiment Setup	58
Figure 7.10 Voltage-Time Graph of Final Experiment	59
Figure 7.11 Voltage-Frequency Graph of Final Experiment	60
Figure 7.12 Comparison of FE Analysis and Final Experiment Results	61
Figure 8.1 Voltage-Time Graph of Helicopter Vibration Profile	63
Figure 8.2 Classified Helicopter Vibration Profile Energy Harvesting.....	63
Figure 8.3 Voltage-Time Graph of Gun Fire Vibration Profile.....	64
Figure 8.4 Classified Gun Fire Vibration Profile Energy Harvesting	65
Figure 8.5 Voltage-Time Graph of Different Vibration Profile	66
Figure 8.6 Voltage-Frequency Graph of Different Vibration Profile.....	66
Figure 8.7 Customized Material CP vs Steel CP Energy Harvesting.....	68

LIST OF TABLES

Table 2.1 Comparison of Wire Rope and Rubber-Elastomer Isolators.....	6
Table 2.2 Comparison of Piezoelectric Materials Properties [21]	10
Table 4.1 Aluminum 6061-T6 Material Properties	18
Table 4.2 Stainless Steel Dummy Mass Material Properties	18
Table 4.3 Dummy Mass Modes	19
Table 4.4 Software and Equipment of Isolator Verification Experiment	23
Table 4.5 Input Vibration Profile	23
Table 4.6 Natural Frequency and Damping Ratio Changes	28
Table 4.7 Comparison of Experiment gRMS Values for Each Isolator	30
Table 5.1 Material Properties of Sheet Metal	32
Table 5.2 First Two Modes of Curved Panel	37
Table 6.1 Mesh Sizing.....	42
Table 6.2 FE Model Natural Frequencies	45
Table 6.3 Analysis vs. Test Result	46
Table 7.1 Isolated FE Model Natural Frequencies.....	48
Table 7.2 Piezoelectric Patch Covered Angle Voltage Data.....	51
Table 7.3 Piezoelectric Patch Covered Angle VRMS Density Data.....	52
Table 7.4 Curved Panel-WRI Stiffness Ratio	54
Table 7.5 Piezoelectric Patch Width Energy Density Data.....	55
Table 7.6 Piezoelectric Patch Thickness Energy Density Data	57
Table 7.7 FE Analysis and Final Experiment Generated Energy Data	62
Table 8.1 MFC Experiment Generated Energy	67
Table 8.2 Customized Material CP vs Steel CP.....	68

LIST OF SYMBOLS AND ABBREVIATIONS

- List of Symbols

V	: Voltage
Q	: Electrical Charge
m	: Mass
f	: Frequency
ζ_e	: Electrical Damping Ratio
C	: Damping Constant
m_{eq}	: Equivalent Mass
K	: Stiffness Constant
ε	: Dielectric Constant
ω_n	: Natural Frequency
ω_d	: Damped Natural Frequency
ζ_m	: Mechanical Damping Ratio
y	: Base Excitation
Y	: Base Displacement
X	: Mass Position
ϕ	: Phase Angle
T	: Time
ω	: Excitation Frequency
f_n	: Resonant Frequency
ζ	: Damping Ratio
D	: Electric Displacement
d_{ij}	: Piezoelectric Modulus
T	: Mechanical Stress
E	: Electric Field
I	: Electric Field Direction
J	: Mechanical Field Direction
T	: Piezoelectric Material Thickness
A_p	: Piezoelectric Material Surface Area
F	: Force
C	: Capacitance

V_p : Piezoelectric Voltage

- List of Abbreviations

FE : Finite Element

FFT : Fast Fourier Transform

PSD : Power Spectral Density

RMS : Root Mean Square

gRMS : Root Mean Square of Acceleration

EH : Energy Harvesting

EHS : Energy Harvesting System

SDOF : Single Degree of Freedom

EI : Elastomer Isolator

WRI : Wire Rope Isolator

APDL : Ansys Parametric Design Language

MAPDL : Mechanical Ansys Parametric Design Language

CP : Curved Panel

EH : Energy Harvesting

VIEH : Vibration Isolation and Energy Harvesting

MEMS : Microelectromechanical Systems

PVDF : Polyvinylidene Fluoride

PZT : Lead Zirconate Titanate

PDMS : Polydimethylsiloxane

PMN : Lead Magnesium Niobate

MFC : Macro-Fiber Composite

1. INTRODUCTION

All electronic devices have an indispensable place in our lives. However, the usage areas and the number of users is increasing day by day. With the widespread use of its use, many studies have been carried out to provide the energy they need for their work. The problem has been overcome for a while by using battery technologies. However, while manpower is needed for the replacement and charging of batteries, devices that can produce their own energy are of greater interest due to the difficulty of manufacturing and recycling and high costs of batteries. It has an important role in the preference of not needing an external power source and battery renewal. Due to these features, self-sufficient devices are preferred especially in areas that are difficult to reach.

Considering the systems that can produce their own energy, they benefit from natural energy sources such as sun, wind, heat and mechanical vibration. While large surface areas are required for the energy produced by using solar energy, the weather conditions must also be suitable. In the generation of energy from wind, large surfaces and high amount of air flow are needed. In the production of energy with heat, large temperature differences are needed. For this reason, energy production by these methods is not preferred in narrow areas and closed areas. Mechanical vibration is the most ideal source to meet the energy needs of small electronic systems.

The most common method used to generate electricity by utilizing vibration is piezoelectric material. Piezoelectric materials create electrical charges against the stress applied on them. In vibration-induced mechanical movements, energy is harvested under high excitation by placing it in places where the movement is intense. Piezoelectric materials are widely preferred in self-sufficient devices due to their ability to be produced in desired sizes and shapes, not requiring additional power sources, having unlimited life under appropriate conditions, and high-power density.

1.1. Motivation

Piezoelectric energy harvesting is done by creating electrical charges on the conductive surfaces as a result of stress formation between the two conductive surfaces of the piezoelectric material. When placed on surfaces where vibration generates intense excitation, stress and energy generation occur at the vibration frequency. As a result of the overlapping of the vibration frequency with the natural frequencies of the harvesting system, high energy outputs occur under high excitation.

In this thesis study, unlike other studies in the literature, energy harvesting is done with PVDF material to be attached to the curved panels to be added to the passive isolator system. This system, which is planned to be used in health monitoring in aircraft with broad frequency band and vibration profile, consists of dummy mass, isolator, curved panel and piezoelectric patches. The curved panel is placed on the base of the isolator and the mass bonding surface. By adhered piezoelectric materials on it, the energy harvesting frequency band is further expanded thanks to the natural frequencies of both the isolator system and the curved panel during vibration. Sensitivity analyses are made in different configurations by changing the dimensions of the curved panel and the piezoelectric material. Thus, the efficiency of energy production and electricity output are increased.

1.2. Scope of the Thesis

In many military platforms, especially in aerial platforms, vibration occurs randomly in broadband (from 0 to 1000 Hz) and at different amplitudes. Due to the high cost and strategic importance of the electronic units installed on this platform, great importance is attached to maintenance and repairs.

These systems are connected with an isolator so that they are less damaged during application. With the energy harvesting system to be placed in the isolators, it is aimed to carry out critical measurements such as health monitoring, vibration measurements, temperature measurements without the need for an additional energy source. In this way, it is aimed to prevent catastrophic damages and to eliminate the need for large and heavy power sources for acceleration or thermal measurements to be made in the field.

1.3. Thesis Outline

This thesis consists of nine chapters. The general contents of the sections are explained below.

The second part contains energy harvesting systems, vibration isolators, piezoelectric material types, curved panel energy harvesting research, vibration isolation and energy harvesting studies in the literature. Evaluations were made in terms of advantages and disadvantages.

The third chapter include analytical models used in isolator selection and piezoelectric energy harvesting. Vibration profiles and design considerations are explained. Due to the changes in the electro-mechanical properties of the piezoelectric patches adhered to the

curved panel, it has become difficult to construct the model analytically. For this reason, the numerical model was used. Since both mechanical and electrical are present in the numerical model, a finite element model that provides a multi-physics solution is needed. For this, Ansys Mechanical APDL Multiphysics program was used. Since there are many materials with nonlinear behavior in the energy harvesting system to be created, the models were established in a simple form by making approaches.

In the fourth chapter, the experimental system of the electronic unit to be integrated into the aircraft was created, and its isolators were selected accordingly. The behavior of the system under random vibration drive with two different types of isolators was investigated under different vibration profiles. The points to be considered while creating the experimental system are explained. Data such as natural frequency and damping ratio were calculated from the obtained data and their behavior against the vibration profile was examined. As a result of the calculations, the vibration profile that will affect the energy harvesting system has been obtained for use in further studies.

The fifth chapter involves energy harvesting experiment on the curved panel. PVDF thin films with the thin steel backing layer were adhered to the determined areas on the curved panel. Sine sweep vibration excitation has been applied to the curved panel and the characteristic natural frequencies of the curved panel have been obtained through the electrical charge formation on the piezoelectric material. Voltage-frequency graphs were obtained for use in verification. Moreover, energy generation from different piezoelectric materials, MFC, was tested with the same experimental test setup and the results were compared.

In the sixth chapter, the finite element model was created using SpaceClaim. Similar boundary conditions were applied and the energy output obtained in the experiment was tried to be obtained. By making mesh sensitivity analysis, analyzes on the optimum mesh size were carried out using Ansys Mechanical APDL Multiphysics. Test results and analysis results were compared and the analysis model was verified with the experiment.

In the seventh chapter, size sensitivity analyses of PVDF piezoelectric patches used in energy harvesting were made according to their regions. The length, width and thickness of the patches were changed respectively. The vibration profile obtained from the isolator verification study was applied in the analysis. Thus, the energy to be obtained when placed between the isolator between the curved panel has been simulated.

The eighth chapter presents different case studies. Shape sensitivity and curved panel mode sensitivity analysis for energy production enhancement were performed and the results were examined.

In the last part, all the studies were briefly evaluated and analyzed.

2. LITERATURE SURVEY

In this section, previous studies on energy harvesting, passive isolation, and isolator systems used with energy harvesting are examined. The materials to be used in the experiment were evaluated in terms of their suitability for the needs and selections were made.

2.1. Vibration Isolation

In military air vehicle, high-frequency vibration occurs in the broadband, depending on the altitude, weather conditions, the weapon systems that is used and the operating frequencies of their engines. A mechanical or electronic failure that may occur in these vehicles with high costs will have vital consequences. The same situation exists in the helicopter, and designing an electronic device (mission computer, radar, radio etc.) that can withstand high accelerations is mechanically challenging due to requirements such as placement in tight spaces and low weight. This vibration, which affects electronic devices, is completely waste of energy that unintentionally created by rotating parts or weapons of air vehicle.

Many precautions have been applied to prevent unwanted vibrations. The most conventional of them is to place a vibration isolator between the vibration source and the load which shown in Figure 2.1. Thanks to the isolators, instantaneous high accelerations and vibrations are transferred to the electronic device by damping, so the usage times of the electronic and mechanical parts of the device will be greatly increased. The absorbed energy is converted into heat with the help of a damper [1] .

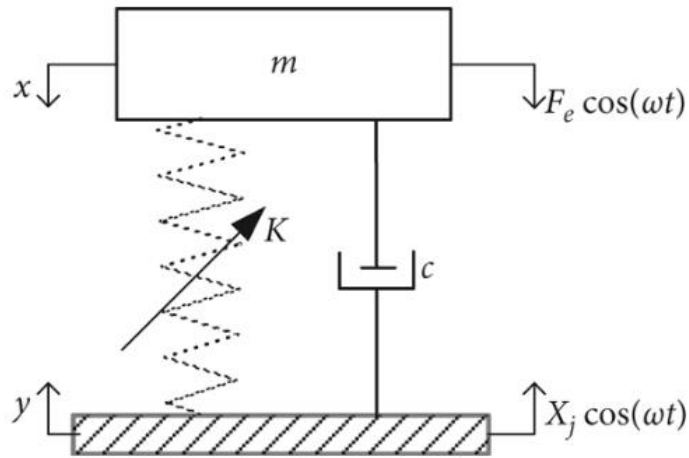


Figure 2.1 Conventional Vibration Isolation

Isolators are divided into two parts, passive and active. Active isolators apply excitation in the opposite direction of the incoming excitation, preventing the connected product from being affected by the movement coming from the base. However, the extra exciter and controllers in the system to be installed complicate the system and greatly increase its cost. An active vibration isolation system model is shown in the Figure 2.2. In passive isolation, only isolators are used. These isolators transfer the vibration to the product by greatly reducing the vibration to be transferred with the damper and spring system placed between the two connection surfaces. The damper and the spring can be separate parts, or the same effect can be created by using materials such as rubber, elastomer and wire rope with damping properties. These isolators provide great convenience in narrow spaces and light product; therefore, they are often preferred [2-4]

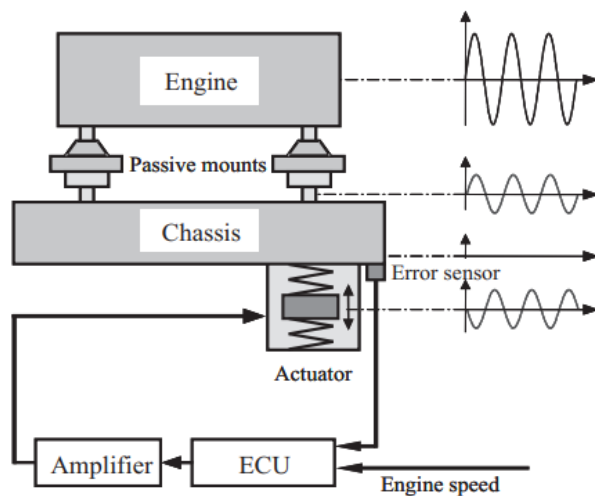


Figure 2.2 Active Vibration Isolation [4]

Elastomer isolators can take many shapes according to the needs, mass production can be made from molds, they can have different damping ratio values according to the material used, and they have high deflection capacity [5].

Wire rope isolators have a fixed shape due to their damping mechanism and their damping ratio can only be up to 0.2. However, compared to others, they have a longer usage period, they are easy to store, their spring stiffness values are more reliable, and their chemical and thermal resistance is quite high [6]. The comparison of the two isolator types is given in the Table 2.1 and the samples are shown in the Figure 2.3.

Table 2.1 Comparison of Wire Rope and Rubber-Elastomer Isolators

Properties	Wire rope isolator	Rubber isolator
Life	+	-
Reliable Stiffness	+	-
Damping ratio	-	+
Deflection capacity	+	+
Chemical strength	+	-
Thermal strength	+	-



Figure 2.3 Vibration Isolators:

a) Wire Rope Isolator, b) Elastomer Isolator

2.2. Energy Harvesting

As the technology develops, the number of technological devices used and technology dependency increase proportionally. However, more energy needs arise and different ways are sought for energy generation. It is tried to benefit as much as possible from the sun, wind, mechanical vibration, radio waves and thermal, which are major energy sources [7, 8].

Since the energy obtained from the sun and wind depends on environmental conditions and needs large surface areas, it is not preferred in small devices such as sensors. Very high temperature differences are needed in thermal energy harvesting. Radio waves require very high wavelengths and can cause disturbance to the environment [8, 9].

Vibration, which is independent of environmental conditions from these sources, is easily accessible and can be encountered in daily life. It can be observed in the entire cyclical movement environment; car, washing machine, heartbeat, walking etc. Energy can be harvested from vibrational energy using three principal mechanisms. They can be listed as electromagnetic, electrostatic, and piezoelectric [7, 10, 11].

The models of the mechanical vibration-based energy harvesting system are shown in the Figure 2.4.

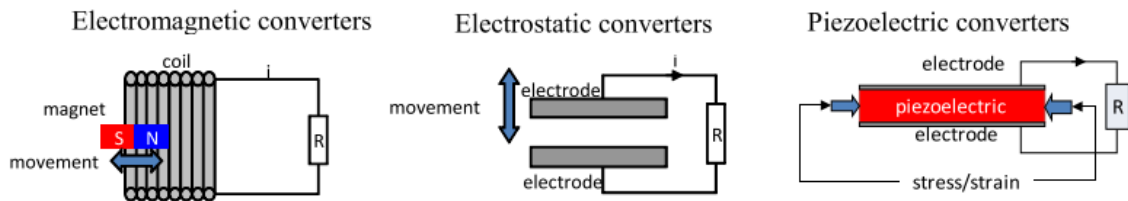


Figure 2.4 Mechanical Vibration Based Energy Harvesting Systems [12]

Electromagnetic energy harvesting works with the principle of electromagnetic induction. The movement of the magnet placed between the coil causes a change in the magnetic field and voltage is obtained in the system with induction current [13]. This harvester model is given in the Figure 2.5.

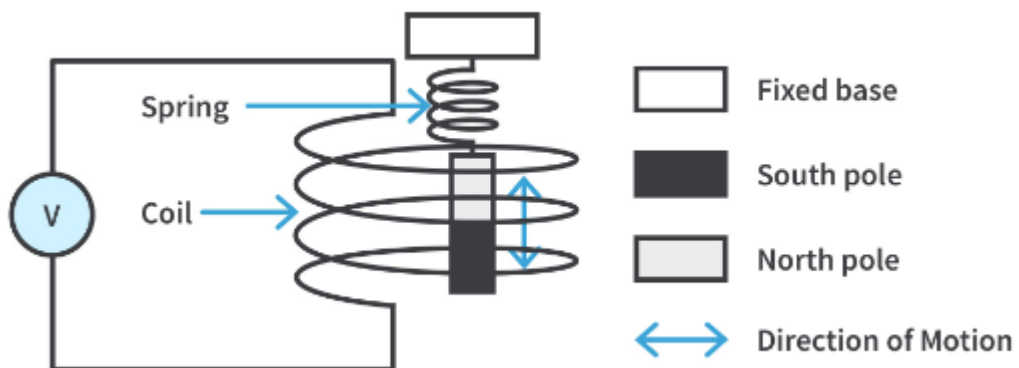


Figure 2.5 Electromagnetic Energy Harvester [14]

Electrostatic energy harvesting is achieved as a result of the change in capacitance of variable capacitors. Voltage generation occurs thanks to the movement of the electrodes it has relative to each other under the effect of vibration [15]. An electrostatic energy harvesting system sample shown in Figure 2.6.

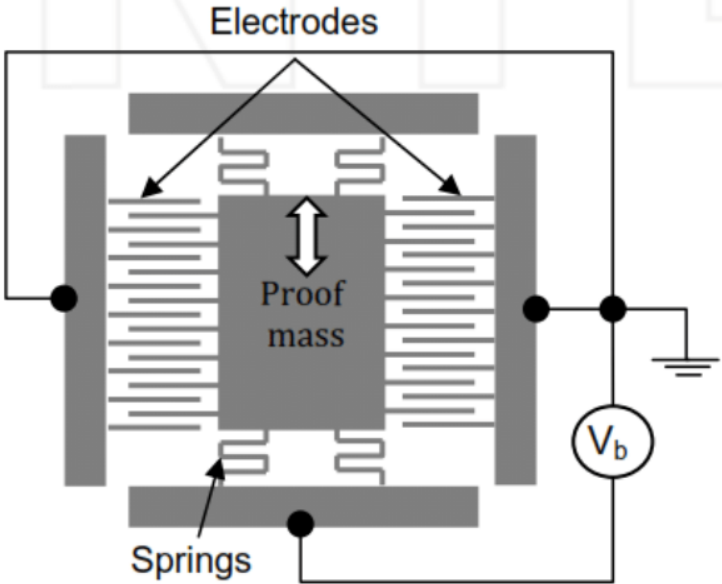


Figure 2.6 Electrostatic Energy Harvester [16]

Piezoelectric material can generate electrical energy if it is strained. This material, placed between the two electrodes, creates variable stress, thereby observing a continuous voltage output [17, 18]. Direct and reverse piezoelectric effect visuals are shown in the Figure 2.7 and Figure 2.8, respectively.

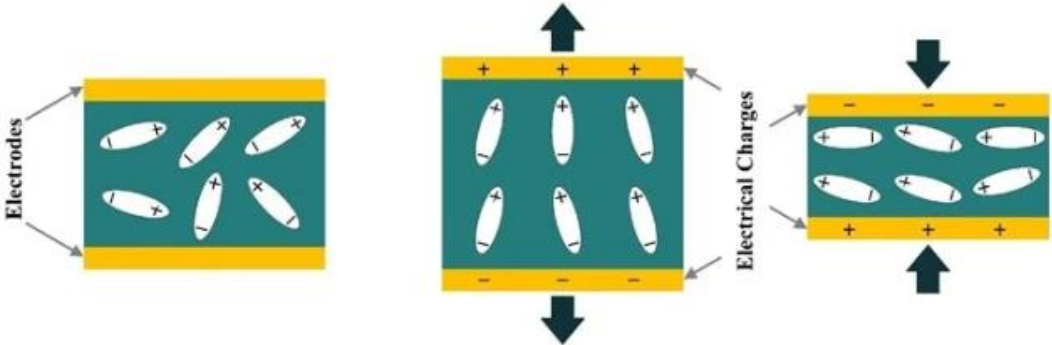


Figure 2.7 Direct Piezoelectric Effect [19]

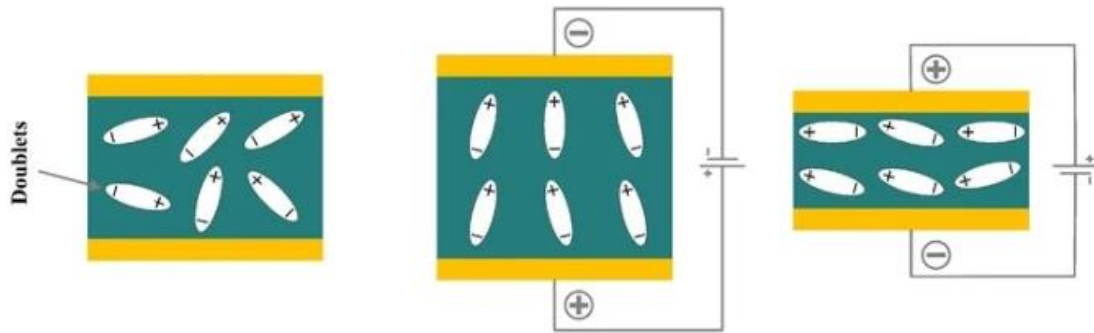


Figure 2.8 Reverse Piezoelectric Effect [19]

In all mechanisms, energy harvesting everlasting thanks to the stress and movements that occur under the variable load acting on them under vibration. The electronic devices can operate in time, which varies according to the size of the power generated. Depending on the energy consumption of the electronic device to be powered by the energy harvesting system, the energy can be used instantly or charged to be used later in the battery or capacitor.

Piezoelectric materials are investigated in four groups according to their structural properties: Piezo-ceramics (Lead zirconate titanate-PZT), Piezo-crystals (lead magnesium niobate-PMN), Piezo-polymers (Polyvinylidene fluoride-PVDF) and Composites. Each material has advantages and disadvantages depending on its properties. The material properties are given in the Table 2.2. The most important property of these materials for energy harvesting is the piezoelectric coupling factor which indicates that the effectiveness of conversion of mechanical energy into electrical energy. Piezo-ceramics provide the highest power output. However, they are fragile due to their ceramic structure, therefore they are not resistant to high loads. The power output of the piezo-crystal is close to piezo-ceramic, but it is not preferred due to its high cost. The piezoelectric material that provides the least electrical energy is the piezoelectric polymers. On the other hand, owing to their high flexibility they can be used on curved surfaces without permanent damage. Since it has low density and elastic modulus, it can be placed in the system without adding extra weight and stiffness [20-22].

Table 2.2 Comparison of Piezoelectric Materials Properties [21]

Properties	PVDF (polymer)	PZT-5H (ceramic)	PMN-32PT (single crystal)	PZT-polymer composite (30% PZT)
Density (kg/m^3)	1780	7500	8100	3080
Dielectric Constant	6	3250	7000	380
Elastic Modulus (GPa)	2	71,4	20,3	-
Electromechanical Coupling Factor	0.22	0.75	0.93	-
Flexibility	+	-	-	+

In piezoelectric energy harvesting studies, the oscillation frequency and the natural frequency of the energy harvesting system are matched to reach the resonance of the established system and the piezoelectric material is provided to generate high energy with high amplitudes. In most of the studies, high amount of motion and power production have been obtained by vibrating the PVDF and PZT materials at the natural frequency of the beam to which they are attached. In order to work in a broadband frequency, different natural frequencies are obtained by changing the lengths of the beams or the weights attached to their ends Figure 2.9 [23].

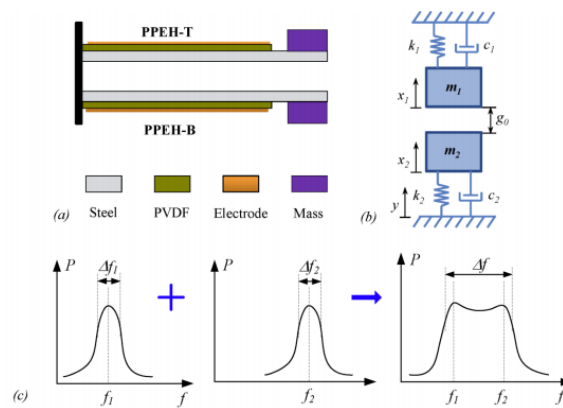


Figure 2.9 Working Frequency Range Change [23]

In another study to increase the frequency range, the natural frequency of the system was kept in continuous resonance by adjusting the position of the load with the actuator connected to the beam end according to the applied vibration frequency. Thus, the system generated energy at higher power with the help of the actuator it operated with the help of its own energy [24].

In order to increase the power generated by the beams working in resonance, efficiency improvement studies were carried out by changing the shapes of the beams [25-27]. It has been observed that when PVDF material is bonded to the curved beam to create prestress

on it, it generates higher power than the flat beam of the same dimensions. The energy harvesting system, which has two half tubes given in Figure 2.10, can generate up to four times the power compared to the flat beam [27]. Two pieces can be placed both above and below the beam due to the low stiffness of the PVDF. The power generated from the same system is doubled Figure 2.10 [23, 28, 29].

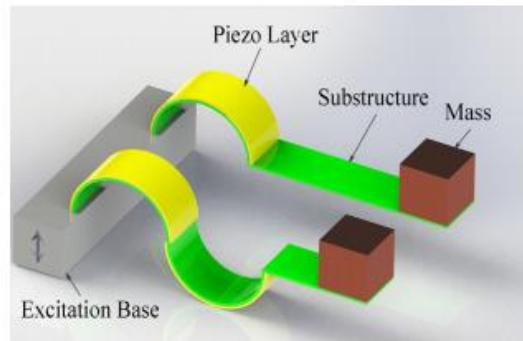


Figure 2.10 Curved Panel Energy Harvesting System [27]

Placement and size studies of PVDF patches have been carried out to improve the increased efficiency by placing them on thin curved panels. Here, by investigating the connection aspects of patches exposed to stress and releases at the same time, the efficiency has been greatly increased by preventing the negative and positive voltage values generated from affecting each other negatively. As a result, it has been observed that the PVDF patches attached to the fixed ends of the curved panels and the ones attached to the middle generate voltage in the opposite direction and the power generated when reversed is increased [26, 30].

2.3. Vibration Isolation and Energy Harvesting

There are also studies in which vibration isolation and energy harvesting (VIEH) systems are used together which is shown in Figure 2.11. VIEH systems are mostly based on harvesting energy with the help of magnetic field. Damping is provided by the damper and spring properties of the materials used in the installed mechanisms. The oscillation continues until the system is damped; thus, voltage output is obtained by changing the electric field of the magnet in the coil [31]. In some studies, energy harvesting was carried out with PVDF bonded on the leaf spring, which provides also isolation [32].

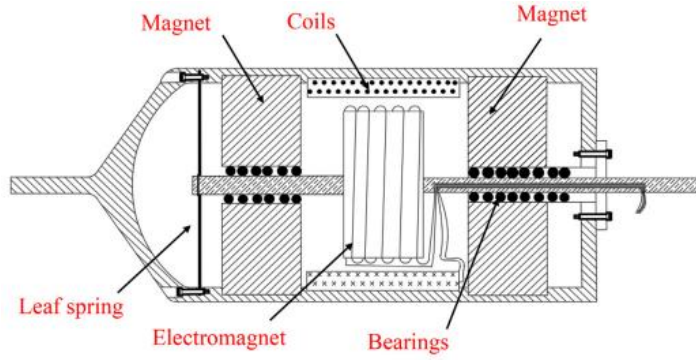


Figure 2.11 Vibration Isolation and Energy Harvesting (VIEH) System Sample [31]

3. THEORY

3.1. Vibration Isolation

Vibrations occurring in high amplitude and wide band in aircraft are attenuated with the help of isolators. Devices, such as the gentle electronic devices, are mounted with the help of four isolators in order to balance the weight. If the weight balance is provided, the system is simply a single degree of freedom (SDOF) base excitation problem. Basic model of SDOF base excited damped system is shown in Figure 3.1.

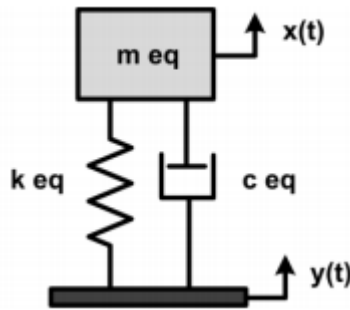


Figure 3.1 SDOF Damped Base Excitation

The equation of motion of the model set up as in the Figure 3.1 above is set up as follows (1).

$$m_{eq}\ddot{x} + c_{eq}\dot{x} + k_{eq}x = c\dot{y} + ky \quad (1)$$

m_{eq} , c_{eq} and k_{eq} represents the mass to be loaded on a single isolator of the electronic device, the damping coefficient of the isolator and the spring constant of the isolator, respectively. Here it is assumed that the thin PVDF layers to be added to the system do not affect the equivalent spring and damping coefficients.

Assuming basically the excitation function from the base is harmonic and can be given such as:

$$y(t)_h = Y_h e^{i\omega t}. \quad (2)$$

In this equation (2), Y_h , ω and t represent the absolute harmonic base displacement, excitation frequency and time, respectively.

In a mass-damper-spring system, the damping ratio (ζ) is calculated as follows;

$$\zeta = \frac{c}{2\sqrt{km}}, \quad (3)$$

The damping coefficient is defined as c .

The undamped natural frequency (ω_n) and damped natural frequency (ω_d) of the system are calculated by equation (4).

$$\omega_n = \sqrt{\frac{k_{eq}}{m_{eq}}}, \quad \omega_d = \omega_n \sqrt{1 - \zeta^2} \quad (4)$$

Since the system to be used is SDOF damped base excitation, the response equation must be solved as homogeneous (transient response) and particular (steady state response) parts. Since transient response disappears in a long time, it will be neglected in our study as well. In equation (5), the time-dependent response of the system is given.

$$X_0 = \frac{Y_0 \sqrt{\left(1 + \left(\frac{2\zeta\omega}{\omega_n}\right)^2\right)}}{\sqrt{\left(\left(1 - \frac{\omega^2}{\omega_n^2}\right)^2 + \left(\frac{2\zeta\omega}{\omega_n}\right)^2\right)}}, \quad \Phi = \text{atan}\left(\frac{2 * \zeta * \frac{\omega}{\omega_n}}{1 - \left(\frac{\omega}{\omega_n}\right)^2}\right) \quad (5)$$

Time Dependent response of mass: $x(t) = X_0 \sin(\omega t + \Phi)$

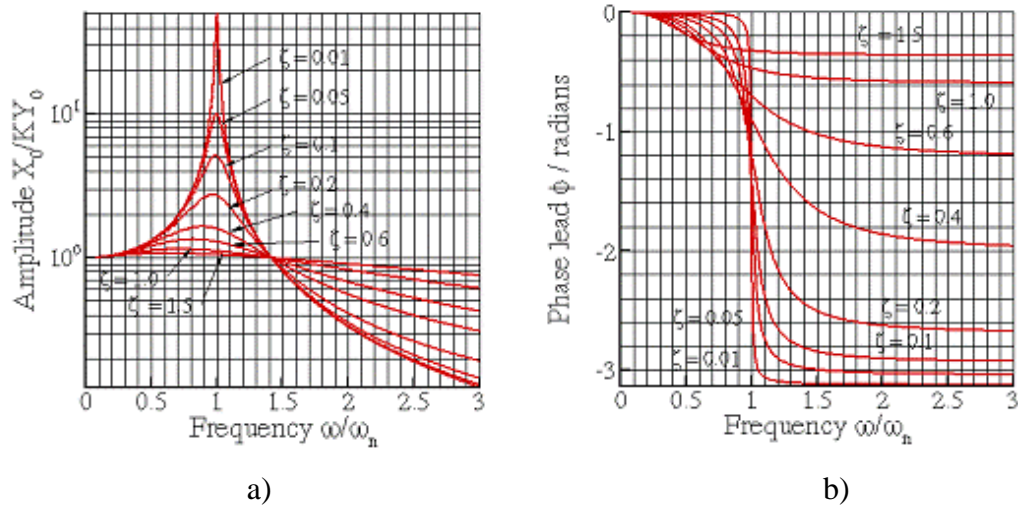


Figure 3.2 SDOF Base Excited System: a) Transmissibility, b) Phase Angle Graphs

The transmissibility is known as the ratio of the amplitude from the base to the mass transfer (X/Y). Phase Angle is considered as the difference between the direction of movement of the base and the direction of movement of the mass. They move together in the same direction when the angle is 0. The transmissibility and phase angle graphs are shown in Figure 3.2.

3.2. Energy Harvesting

Whereby energy will be harvested through the curved panel to be connected between the vibration excitation coming from the base and the connection area of the mass, the relative motion in between will be needed. Therefore, equation (6) should be used to calculate the movement of the curved panel and the amount of energy to be harvested.

$$z(t) = x(t) - y(t)_h \quad (6)$$

The piezoelectric materials are anisotropic. The axes of the piezoelectric material are shown in Figure 3.3, the stress (polarization) direction of the piezoelectric material is chosen as the third axis. The electromechanical equation of the linear piezoelectric material is given in equation (7).

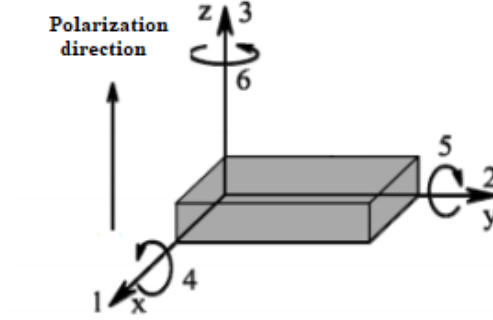


Figure 3.3 Piezoelectric Material Axes and Polarization Direction

$$\begin{bmatrix} D_1 \\ D_2 \\ D_3 \end{bmatrix} = \begin{bmatrix} 0 & 0 & 0 & 0 & d_{15} & 0 \\ 0 & 0 & 0 & d_{24} & 0 & 0 \\ d_{31} & d_{32} & d_{33} & 0 & 0 & 0 \end{bmatrix} \begin{bmatrix} T_1 \\ T_2 \\ T_3 \\ T_4 \\ T_5 \\ T_6 \end{bmatrix} + \begin{bmatrix} \epsilon_{11} & 0 & 0 \\ 0 & \epsilon_{22} & 0 \\ 0 & 0 & \epsilon_{33} \end{bmatrix} \begin{bmatrix} E_1 \\ E_2 \\ E_3 \end{bmatrix} \quad (7)$$

D matrix shows the electric displacement, d_{ij} is the piezoelectric modulus values, T matrix is the mechanical stress, ϵ is the dielectric constants, E is matrix electric field. i and j represent the electric field direction and the mechanical stress direction, respectively. When a force is applied in the same direction as the polarization direction, the equation becomes simpler as in equation (8).

$$D_3 = d_{33}T_3 + \epsilon_{33}E_3 \quad (8)$$

$$T_3 = \frac{F}{A_p}, \quad E_3 = \frac{V_s}{t_p} \quad (9)$$

Mechanical stress and electric field calculations are given in equation (9). Here, F shows the applied force, A_p the surface area, t_p the thickness of the piezoelectric material, V_s the applied potential difference. The amount of charge is calculated as in the q equation (10)

$$q = D_3A_p \quad (10)$$

Equation (11) gives the formula for the capacitance value of the piezoelectric material

$$C = \frac{\epsilon_{33}A_p}{t_p} \quad (11)$$

Consequently, the amount of voltage generated by the piezoelectric material, V_p , is calculated from equation (12).

$$V_p = \frac{q}{C} \quad (12)$$

4. VIBRATION ISOLATOR

Within the scope of piezoelectric energy harvesting experiments with curved panel to be placed on the vibration isolator, two different isolators were studied. One of them is the rubber isolator (RI) and the other is the wire rope isolator (WRI). In the studies, a dummy mass was attached to the isolators, representing the sensitive electronic device that is not to be damaged by vibration. The same dummy mass was used to ensure that the same amount of energy was applied while using the same vibration profiles during the experiments.

In the selection of isolators, care was taken to ensure that the isolators have the desired damping ratio under the same load, the appropriate stiffness value and sufficient displacement so that they do not completely restrict the movement. The elastomer and wire rope isolators chosen for use in the experiment were selected according to their specifications in their manufacturer's catalogues.

Although the same mass is used, the behavior of the isolator's changes depending on the amplitude of the vibration profile due to their nonlinearity. For this reason, working only according to the data which obtained from the isolator catalogs will not give completely accurate results. As a result, vibrations of different amplitudes will be applied to the isolators and the stiffness and damping rates will be found, then the isolator model will be established in the Ansys APDL program and verified.

In order to verify the isolator, a vibration table and mass suitable for the connection interface of the selected isolators to be used in the experimental setup were designed. The same table and mass were used for both isolators in order to complete the experiment under exactly the same conditions.

During the design, special attention was paid to ensure that the natural frequencies of the table and the dummy mass are higher than the excitation frequency. Because if they are excited their natural frequencies during the experiment, the extra movement they will

create will cause the isolators to act with a higher input than the energy given to them then cause us to read an incorrect response.

4.1. Modal Test

Vibration occurs randomly in aircraft and high acceleration values can be obtained even at high frequencies. Since data cannot be obtained from all avionic platforms, studies will be carried out on a helicopter selected with reference to the DO-160G document. Considering the vibration profiles of the helicopter platforms, it is seen that they are significant up to 1000 Hz frequency, which can damage the systems.

4.1.1. Isolator Selection

It is planned to connect the electronic unit, which is planned to be mounted on the platform where random vibration is located, with an isolator so that it is less damaged due to vibration.

A dummy mass will be mounted on the isolators representing the electronic unit. 2.4 kg was determined as the dummy mass weight and isolator selections were made accordingly. In the selection of the isolator, the natural frequency of the system has been tried to be kept as low as possible. Because the input vibration given at frequency $\sqrt{2}$ times after its resonance, which will occur at low frequencies, will be greatly damped and the input energy will turn into relative motion between the base and the mass. Thus, the curved panel, which is our energy harvesting system, will vibrate and allow a high rate of energy harvesting.

4.1.2. Vibration Table Design

The shaker and isolators must have a connection interface on the vibration table. After the fixed shaker connection interface was drilled to the table, the connection interface of the isolators was also attached to the table.

The natural frequencies of the table were found using the Modal analysis tool of Ansys Workbench. While establishing the analysis model, the surfaces that the table connects to the shaker are defined as fixed to the ground. The interface to which the isolators will be connected is defined as the point mass by calculating the dummy mass on it and the mass of the isolators. During the experiment, vibration will be applied to the whole system only in the vertical axis. Therefore, in order to allow the table to move only vertically during the analysis, 0 displacement is defined in the X and Y axes and free in the Z axis. When

modal analysis is performed, it is aimed to have the first natural frequency lower than 1000 Hz. After the material assignments were made, modal analyzes were made. While determining the material, attention was paid to its low cost, easy access and easy processing. The material properties of the vibration table are given in the Table 4.1

Table 4.1 Aluminum 6061-T6 Material Properties

Density	2849 <i>kg/m³</i>
Young's Modulus	68.9 <i>GPa</i>
Poission's Ratio	0.33
Ultimate Tensile Strength	310 <i>MPa</i>
Yield Strength	276 <i>MPa</i>

4.1.3. Dummy Mass Design

In the dummy mass design, after two different isolators are placed on the vibration table, the minimum width and depth dimensions are determined in the frame of the upper connection points of the isolators. In order to reach 2.4 kg, which is the estimated weight in the selection of the isolator, height estimations were made using various materials. The modal analysis was performed by determining the Free-Free boundary condition. The material properties of the dummy mass are given in the Table 4.2.

Table 4.2 Stainless Steel Dummy Mass Material Properties

Density	8000 <i>kg/m³</i>
Young's Modulus	205 <i>GPa</i>
Poission's Ratio	0.27
Ultimate Tensile Strength	580 <i>MPa</i>
Yield Strength	290 <i>MPa</i>

The first 6 natural frequencies will be very low because we do not restrict the boundary conditions. Ignoring these very low first 6 modes which called as free body motion, the next natural frequencies should be above 1000 Hz. After the first six rigid body motion mode of mass, the first mode shape shown in Figure 4.1. As a result of modal analysis, modes of dummy mass given below in Table 4.3.

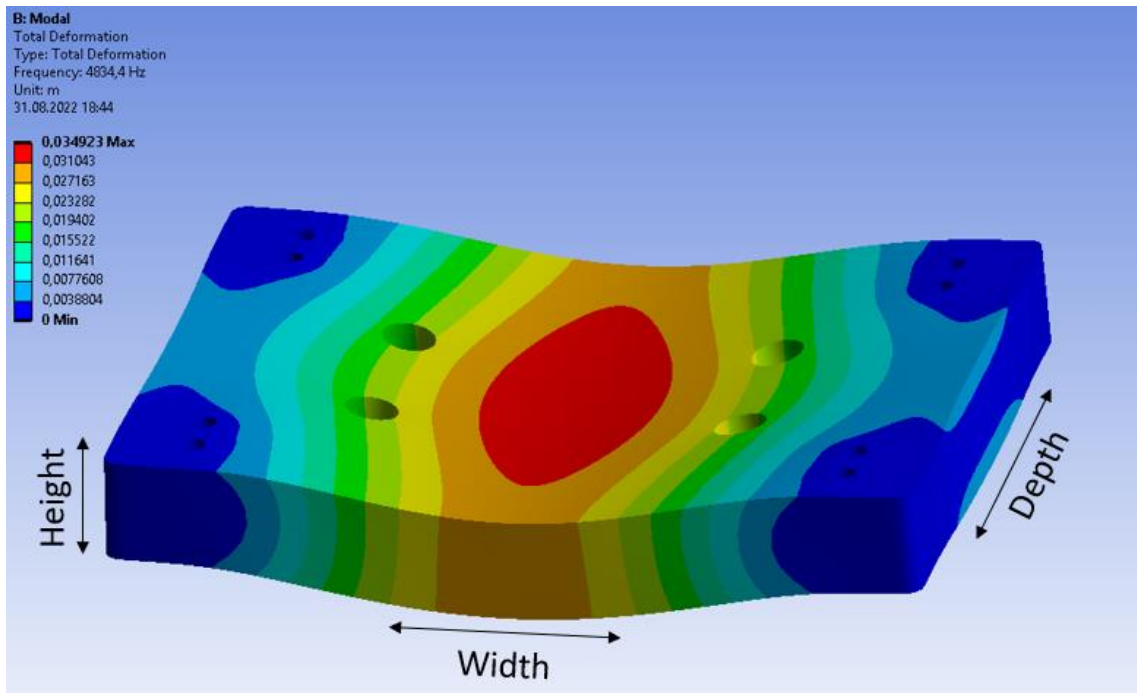


Figure 4.1 1st mode of Dummy Mass

Table 4.3 Dummy Mass Modes

Modes	Frequency [Hz]
1-6	0
7	4834.4
8	6644.9
9	10058
10	10766

4.2. Test Setup

After producing the vibration table and dummy mass designs, an experimental setup was set up to see the natural frequencies and behaviors of the system.

The vibration table is fixed to the Shaker with 16 pieces M10 screws. During screwing, all screws are placed in order to avoid any gaps with the shaker in some parts of the table, and first the opposing screws are fixed with low torque and then the fastening is completed with high torque.

It is aimed to be fixed completely by using a large number of screws. Since there are more screws in the center of the table and the distance between the screws increases as the radius increases, the probability of strain will increase in the table, so the isolators to be

connected should be close to the center. Thus, the vibration table can be applied from the bases of the isolators as well as the input taken from the shaker.

Each rubber isolator is fixed to the vibration table with 4x M5 screws with a torque of 3 Nm. The dummy mass, on the other hand, is torqued to these isolators with a total of 8 screws with 3 Nm and the assembly is completed.

Wire rope isolators are fixed to the table with 4x M5 screws with a torque of 3 Nm. The dummy mass is torqued to Wire rope isolators with a total of 4x M5 screws with 3 Nm and the assembly is completed.

Screws and torque values used in assembly were kept constant and kept under control. Because as the torque values change, the basic behaviors of the systems such as natural frequency and damping ratio change. Such a method was followed in order to avoid system-related inconsistencies during energy harvesting, which is the next stage of the experiments.

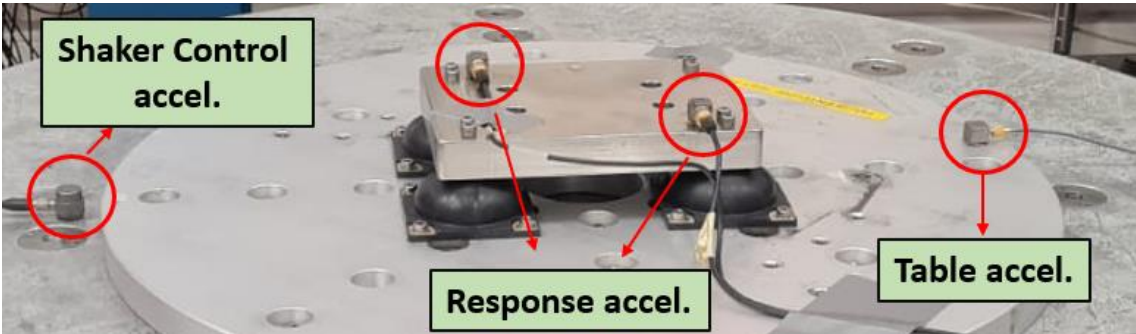


Figure 4.2 A sample picture for the RI test setup

In the test setup, which shown in Figure 4.2, total four 3-axis accelerometers were installed, 2 on the dummy mass and 2 on the vibration table. The accelerometers are fixed on the dummy mass by means of resin at the two diagonal corners in order to see the problems caused by screw connections. If there is no big difference between the accelerometer data behaviors, the studies will be continued by taking the average of the data. If large differences are observed, the experiment will be repeated.

As can be seen in Figure 4.3 and Figure 4.4, since there was no big difference between left and right probes, the studies were continued by taking the average values.

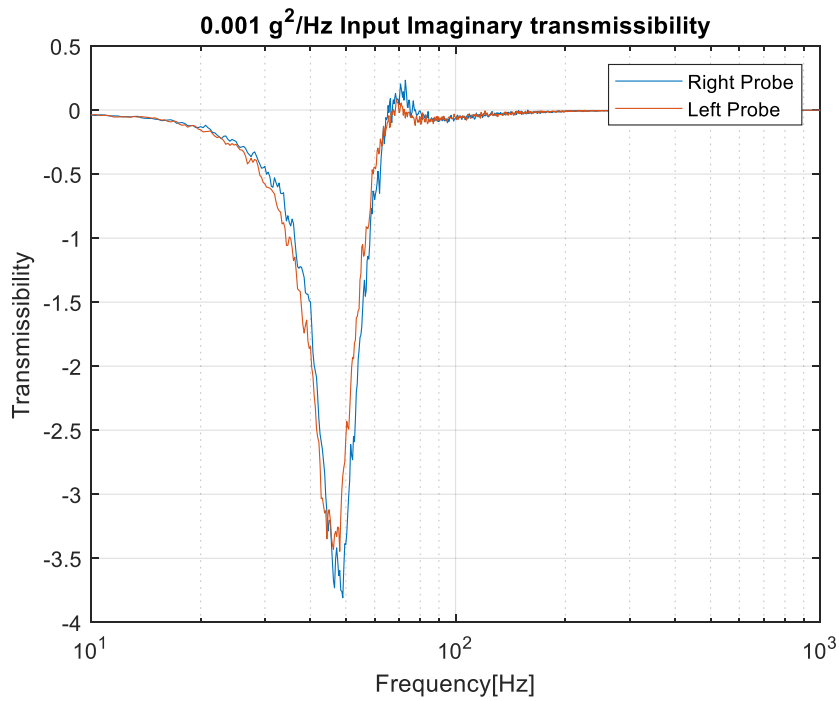


Figure 4.3 Imaginary Transmissibility of Left-Right Accelerometers

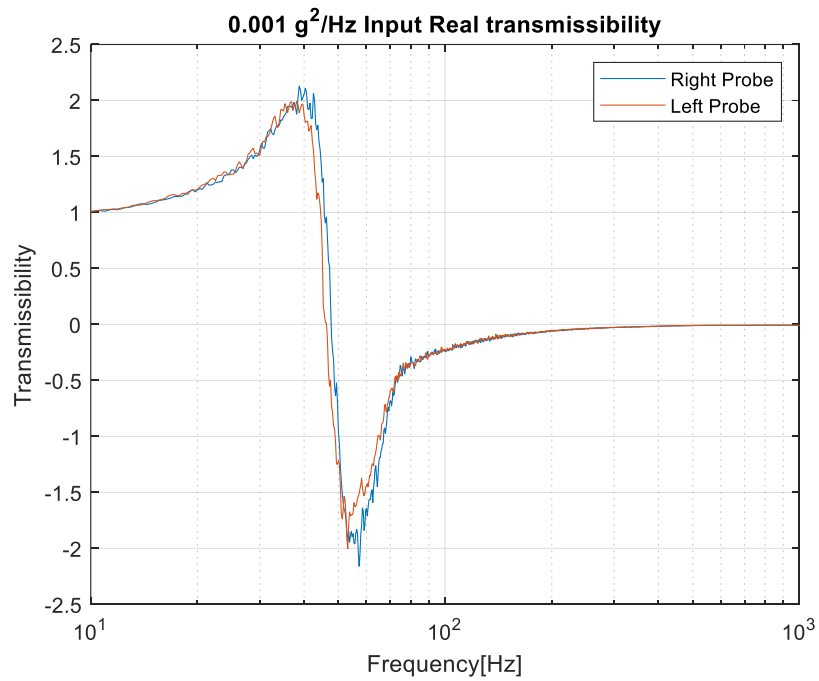


Figure 4.4 Real Transmissibility of Left-Right Accelerometers

One of the accelerometers attached to the vibration table is used as the control sensor of the shaker. Shaker controls the excitation it applies by receiving feedback from this

accelerometer. Thus, power and acceleration losses are prevented during movement and the correctness of the applied vibration is ensured. The other accelerometer on the table is used to measure the applied vibration profile. These data will be used in studies.

In order not to cause extra noise in the data by moving the cables of the accelerometers during vibration and to prevent the resin adhesives from loosening, they are attached to the fixed floor with the help of tape.

4.3. Experiment

The shaker to which the vibration will be applied in the experiment is LDS V8-440. The profile of the applied vibration is defined from the shaker control program, and the data of the control accelerometer is also checked here. According to these data, it automatically manages the amount of excitation and applies the desired vibration profile with a margin of error of 10%. 0.008 g²/Hz white noise vibration profile as an example shown in Figure 4.5.

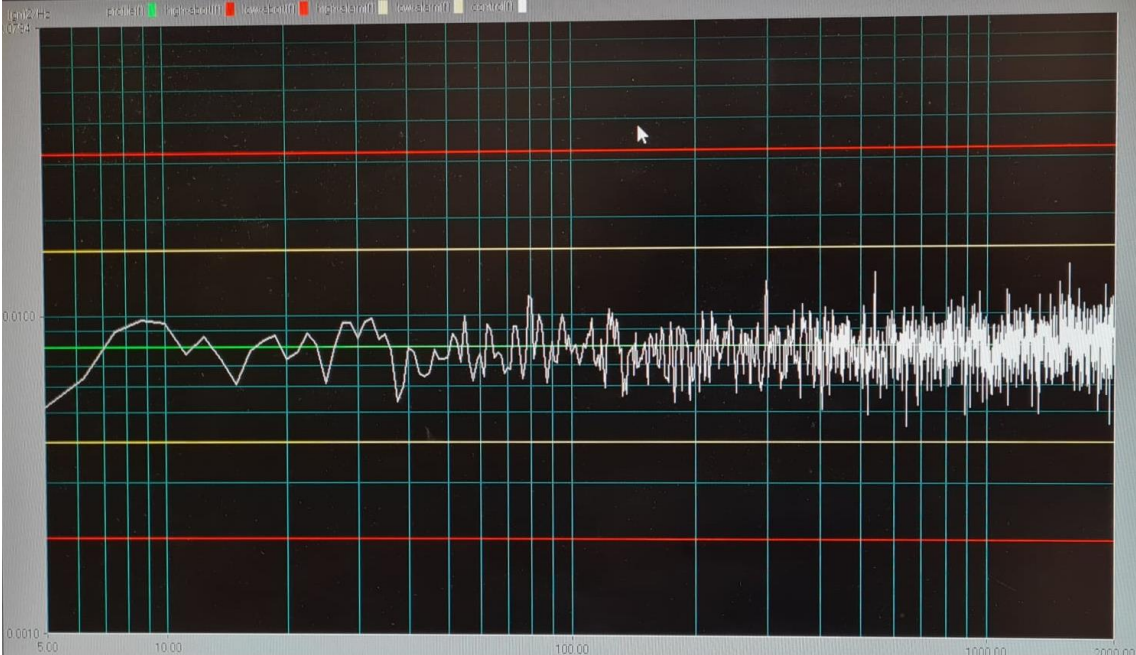


Figure 4.5 White Noise 0.008 g²/Hz

Table 4.4 shows the equipment and software used during the isolator verification experiment.

Table 4.4 Software and Equipment of Isolator Verification Experiment

Software	Pulse Labshop 16.1
Electrodynamic Shaker	LDS V8-440
Data Acquisition Unit	Brüel & Kjaer 3560C
Accelerometers	Brüel & Kjaer Type 4507B and Type 4524B

The table, isolator and mass system connected to the shaker will be excited by white noise random vibration at determined gRMS values for 0-2000 Hz range. When excites with different gRMS values, the behavior of the system will be controlled and their efficiency and effects in energy harvesting studies will be examined. The vibration amplitudes to be applied and gRMS values are shown in the Table 4.5

Table 4.5 Input Vibration Profile

Amplitude of the Input [g²/Hz]	gRMS of the Input
0.001	1.41
0.002	2
0.004	2.83
0.006	3.46
0.008	4
0.02	6.32

Input PSD graphics applied to the system by shaker are shown in the Figure 4.6.

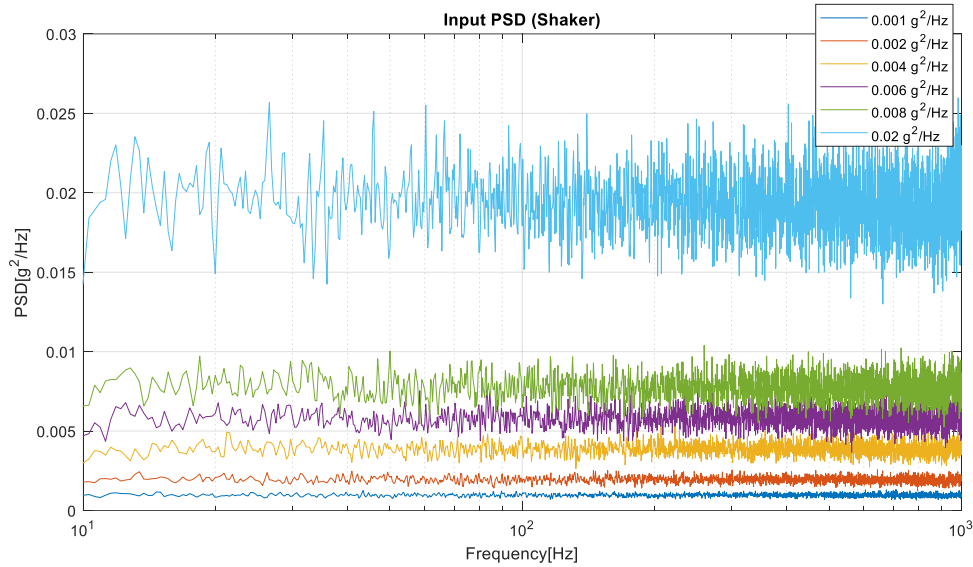


Figure 4.6 Input PSD

The data formed in the accelerometers used in the experiment were obtained by using the Pulse Labshop 16.1. Accelerometers collect data as acceleration in the time domain. Because of the frequency domain is needed in the calculations, the data in the time domain obtained were converted to the frequency domain with 67% overlap with 0.3125 Hz resolution using the MATLAB. Moreover, Hanning window is applied to eliminate the disturbances affecting the system during the test.

Up to 2000 Hz data has been collected, although data up to 1000 Hz is sufficient as high amplitude motion is needed for energy harvesting. As a result, in this frequency range PSD data were used to find natural frequencies and to calculate damping ratio and transmissibility.

4.4. Results

The data obtained as acceleration was taken to be used as harmonic input in the Ansys Mechanical APDL harmonic analysis tool.

As a result of the experiment, when the data obtained from each accelerometer was examined, 3 different values were obtained for each axis: imaginary transmissibility, real transmissibility and magnitude of transmissibility which are shown in Figure 4.7, Figure 4.8 and Figure 4.9 respectively. Thus, the behavior of the system will be obtained and used in analysis studies.

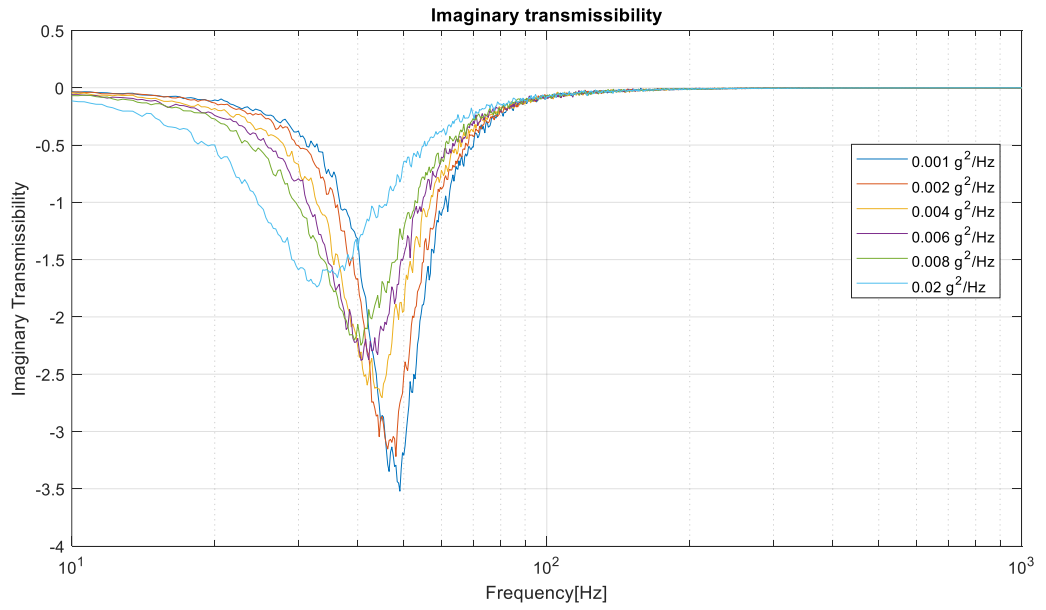


Figure 4.7 Imaginary Transmissibility for WRI

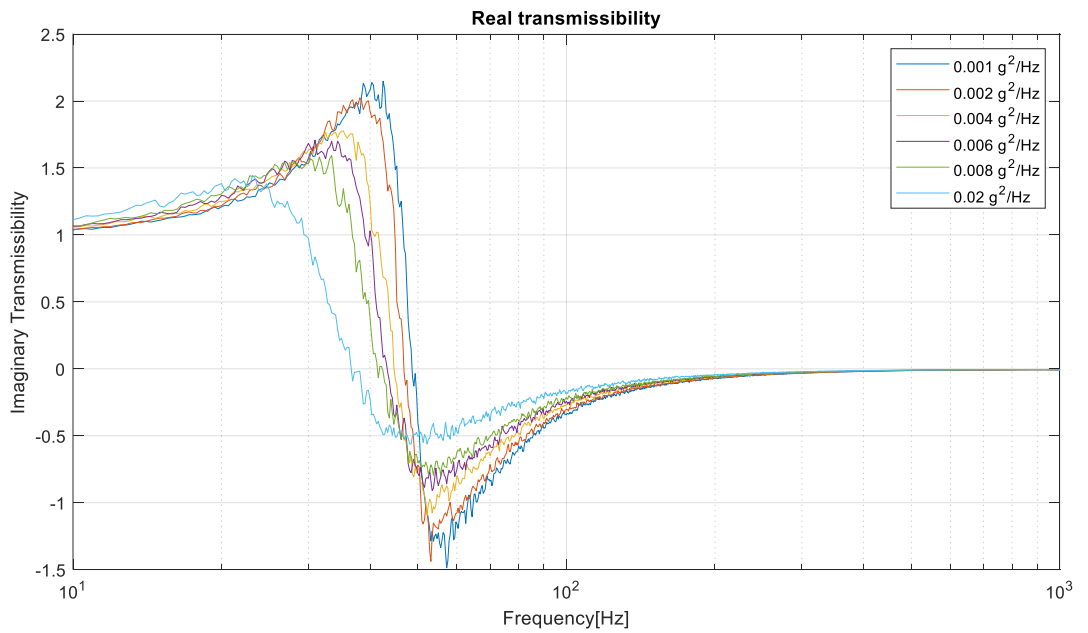


Figure 4.8 Real Transmissibility for WRI

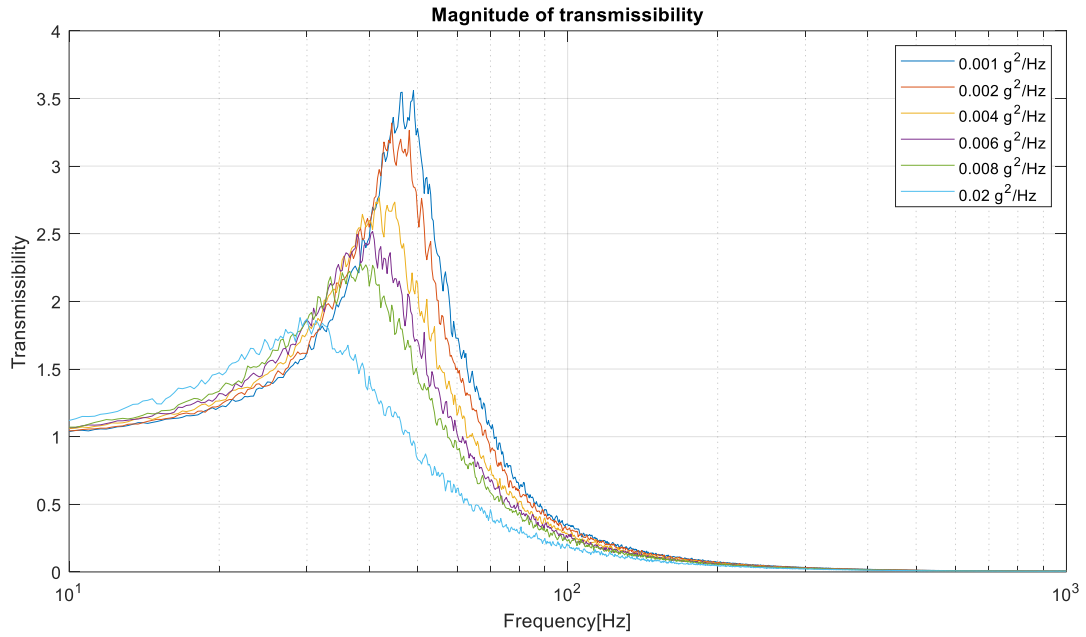


Figure 4.9 Magnitude of Transmissibility for WRI

In the elastomer isolator test, the highest white noise vibration profile ($0.02 \text{ g}^2/\text{Hz}$) could not be applied due to the electrical current problem of the shaker. The magnitude graph obtained with the applied vibration profiles is given in Figure 4.10.

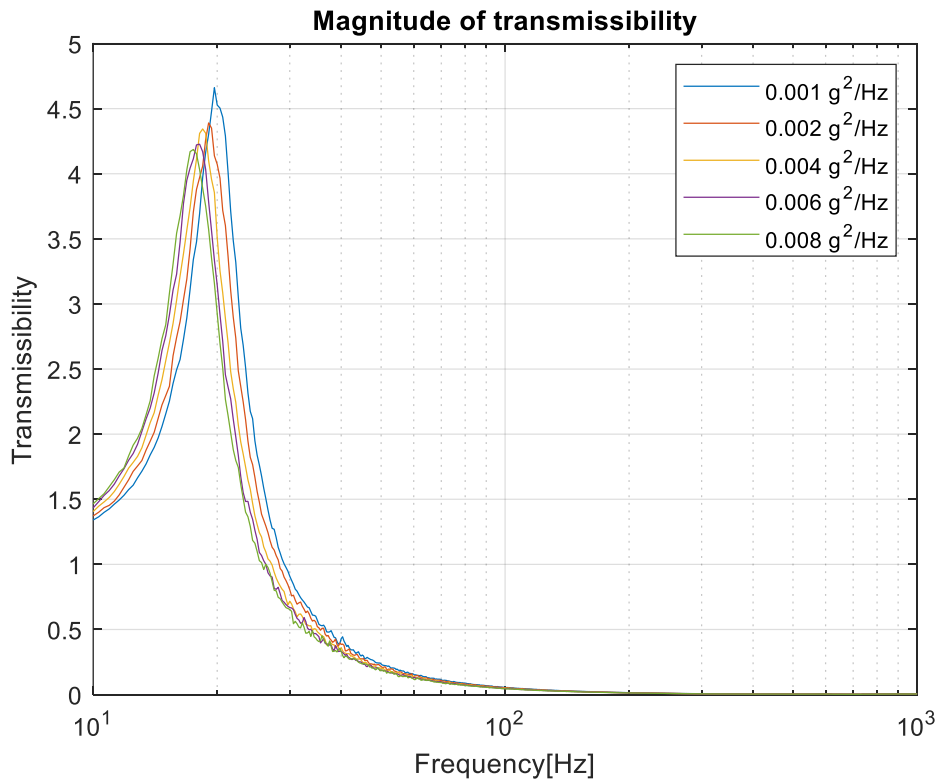


Figure 4.10 Magnitude of Transmissibility for EI

The PSD values of the X and Y axes are quite low compared to the Z axis, as can be shown in the Figure 4.11. For this reason, these axes were ignored in the all calculations.

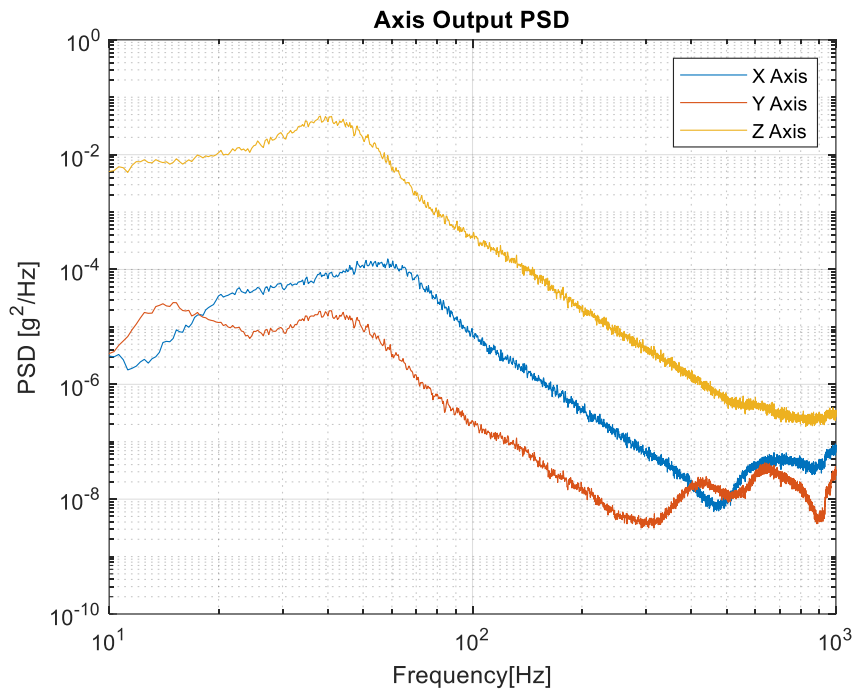


Figure 4.11 Output PSD of Each Axis

Using the peak picking method based on real and imaginary values, natural frequency and damping ratio values can be obtained for each excitation amplitude of the system.

The changes of resulting natural frequency and damping ratio values of wire rope isolator against the input PSD are given in the Figure 4.12 and Figure 4.13 respectively.

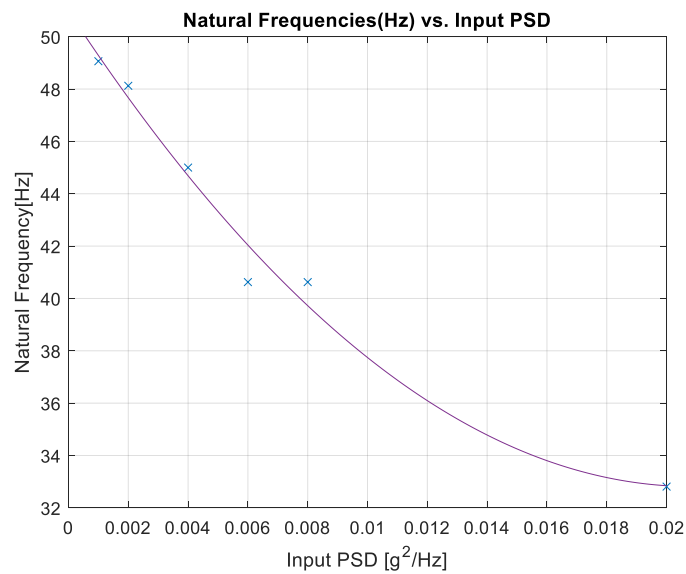


Figure 4.12 Natural Frequency for Each Input PSD of WRI

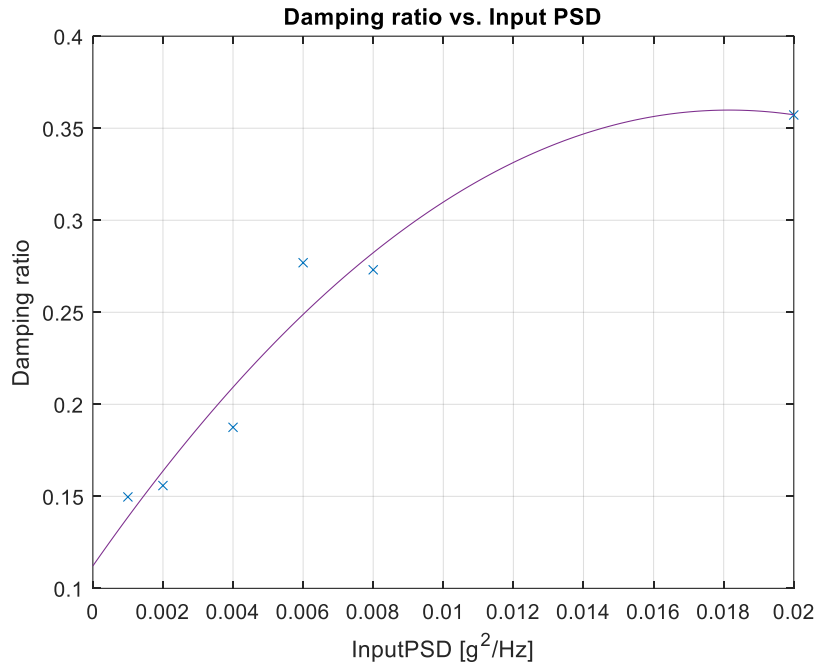


Figure 4.13 Damping Ratio for Each Input PSD of WRI

When WRI and EI are compared, EI natural frequencies show a more linear change in response to input change. However, the damping ratio follows increasing and decreasing trends against increasing input. In the Table 4.6 the values of natural frequencies and damping ratios are given for both isolators.

Table 4.6 Natural Frequency and Damping Ratio Changes

Amplitude of the Input [g^2/Hz]	Natural Frequency of WRI [Hz]	Damping Ratio of WRI, ζ	Natural Frequency of EI [Hz]	Damping Ratio of EI, ζ
0.001	49.06	0.15	20.16	0.132
0.002	48.13	0.156	19.22	0.114
0.004	45	0.188	18.59	0.126
0.006	40.63	0.277	18.28	0.111
0.008	40.63	0.273	17.66	0.124
0.020	32.81	0.357	-	-

As can be seen in the Figure 4.12, the natural frequency of the system decreases inversely as the input values increase. It has high natural frequencies at low excitation amplitudes, while its natural frequency decreases nonlinearly at rising excitation amplitudes.

When the damping ratio graph is examined, as can be seen in the Figure 4.13, when the excitation amplitude is increased, the damping ratio also increases in a nonlinear way for WRI.

While the damping ratios of WRI and EI are close under $0.001 \text{ g}^2/\text{Hz}$ input, the WRI damping ratio reaches higher values as the input value increases. It is clearly seen that EI has values close to the initial damping ratios.

The response graph obtained as a result of the data obtained from the dummy mass in the experiment is given in the Figure 4.14. The natural frequency change according to the input values is also clearly seen in the graph. After $\sqrt{2}$ times the natural frequency, the response value decreases considerably, regardless of the amplitude of the input value.

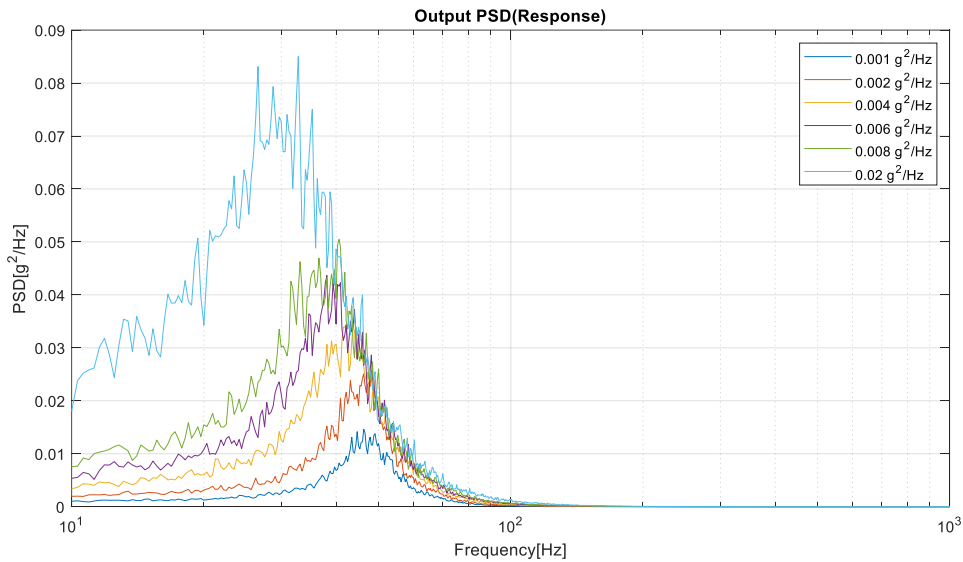


Figure 4.14 Output (Response) PSD of WRI

When the response PSD values are analyzed, it is seen that the input value amplifies near the resonance frequency and reaches much higher amplitude values. This means that high amplitude relative motion will occur between the base of the isolators and the dummy mass at low frequencies due to resonance and at high frequencies due to damping.

By subtracting the input acceleration from the output acceleration, the vibration profile that a curved panel to be connected to the system will be exposed to is obtained which shown in Figure 4.15.

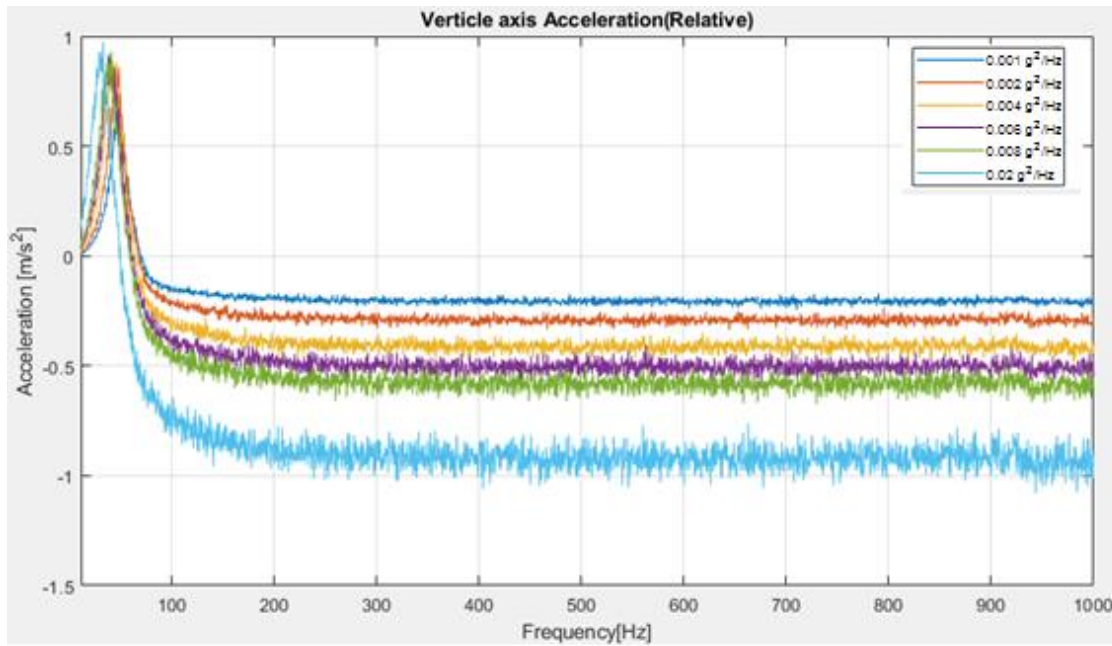


Figure 4.15 Relative Acceleration of WRI

When the gRMS values of the resulting vibration profile is calculated, the Table 4.7 is obtained.

Table 4.7 Comparison of Experiment gRMS Values for Each Isolator

Amplitude of the Input [g ² /Hz]	gRMS of the Shaker	gRMS of Output WRI (Response)	Relative gRMS of WRI <i>output-input</i>	Relative gRMS of EI <i>output-input</i>
0.001	1.38	0.54	1.45	1.4
0.002	1.96	0.73	2.03	1.99
0.004	2.76	0.92	2.83	2.81
0.006	3.38	1.04	3.43	3.44
0.008	3.9	1.14	3.94	3.97
0.020	6.16	1.5	6.17	-

Considering these relative gRMS values, higher energy is obtained from the vibration profile applied to the system of the excitation vibration coming from the isolator system to the curved panel only. With the amplification coming from the natural frequencies of the curved panel up to 1000 Hz, it is expected that higher vibration energy will be applied to the energy harvesting system from the input energy.

When the relative responses of WRI and EI are examined, while WRI generates more energy at low vibration profiles, EI generates energy close to the input energy. In high vibration profiles, while the relative motion energy of WRI approaches the input energy, the energy of EI is much higher.

Thanks to the fact that WRI's height is higher than EI's, it provides a longer and producible experimental setup. At the same time, when the curved panel is connected to the WRI, it has a semicircular shape. Therefore, further studies will be continued with WRI.

5. CURVED PANEL

In order to correctly create the FE model of the curved panel piezoelectric energy harvesting study in Ansys workbench, first of all, the experimental setup must be set up and data must be obtained. Because the piezoelectric patches will be bond on the curved panel, which is the skeleton of the energy harvesting system to be installed. For this reason, prestress will occur on the piezoelectric materials and will significantly change their behavior by affecting the electro-mechanical properties of the materials. As a result, the amount of voltage that the system will produce against the stress that will occur during vibration will be different from what is expected theoretically. By making changes in the structural properties of the piezoelectric material in Ansys MAPDL, the voltage value obtained as a result of the analysis will be tried to equal the voltage values obtained during the experiment.

5.1. Curved Panel Experiment

In the parametric sensitivity study planned for the curved panel energy harvesting system, applying all the parameters to the experimental setup will take a long time and cause high costs. For this reason, an experimental study will be carried out in line with a selected parameter.

The voltage produced in the time domain will be processed and converted into the frequency domain. Thus, it will be possible to compare the FE model results obtained from the Ansys Mechanical APDL Harmonic Analysis tool. As a result of the analysis, the electro-mechanical properties of the piezoelectric material will be changed, and results close to the data obtained from the experiment will be reached.

5.1.1. Curved Panel Specification

The curved panel to be used in the experiment was selected in length to be suitable for the wire rope isolator for ease of production. This length is calculated as the perimeter of the semicircle, with the height of the WRI being the diameter. The surfaces on which it will be mounted are left with an extra length of 10 mm at the both ends. Curved panel width is determined as 8 mm. Material and thickness are preferred as steel sheet metal available in the market.

When the part production is completed, the panel stays flat. Curved shape is provided by connecting the base and top of the isolator. Installation was completed within the framework of these dimensions and the material was grinded to prevent injuries during experiment. The material properties of curved panel are given in Table 5.1.

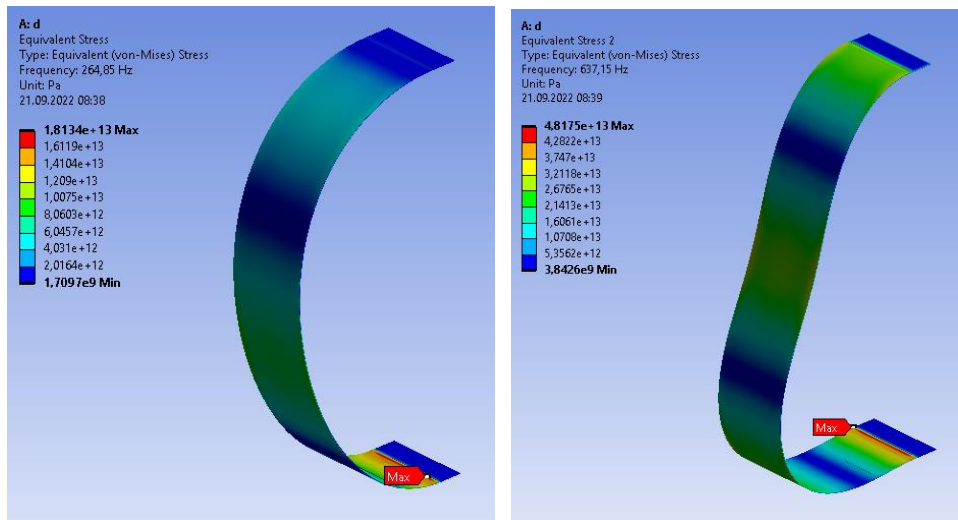
Table 5.1 Material Properties of Sheet Metal

Density	8000 <i>kg/m³</i>
Young's Modulus	190 <i>GPa</i>
Poission's Ratio	0.27
Ultimate Tensile Strength	580 <i>MPa</i>
Yield Strength	290 <i>MPa</i>

5.1.2. Piezoelectric Patch Specification

Piezoelectric patch bonded to the curved panel will be subjected to both compression and tension at the same time. It is not designed as a single piece as the positive and negative charges that will occur on the same patch due to the stress difference can neutralize each other. Instead, with a preliminary study, it is aimed to achieve higher voltage and power density by bonding patches to areas with high stress when force is applied to the panel.

Figure 5.1 shows the first two modes of the curved panel model. In line with the high-stress areas shown, it was decided to use a piezoelectric patch in 3 places, two ends and the middle of the panel. Thus, the formation of phase differences in the voltage values generated will also be observed and the connection directions of the patches to each other will be examined.



a) First Mode

b) Second Mode

Figure 5.1 First Two Modes of FE Model

The patches to be bonded on the curved panel were chosen to cover the 30° angle of the circle whose diameter is the height of the WRI. This configuration was preferred because they are the average value of the parametric angle study to be performed.

Piezoelectric patches, whose dimensions are determined and whose surfaces are covered with conductive material, transmit the voltages generated by 0.2 mm copper cables to prevent them from vibrating at high amplitudes during the experiment and corrupting the data. The cables are adhered to both sides of the patches with a two-component, electrically conductive epoxy containing silver. Since the conductive adhesive becomes solid when cured, it will prevent the piezoelectric patches from generating electricity from their active areas during vibration. For this reason, inactive surfaces have been created in the patches, which will not have a role in electricity generation due to the bonding of the cables and the solidification of the adhesive. Thus, higher accuracy was obtained in the experiment. Piezoelectric patches and inactive areas are shown in Figure 5.2.

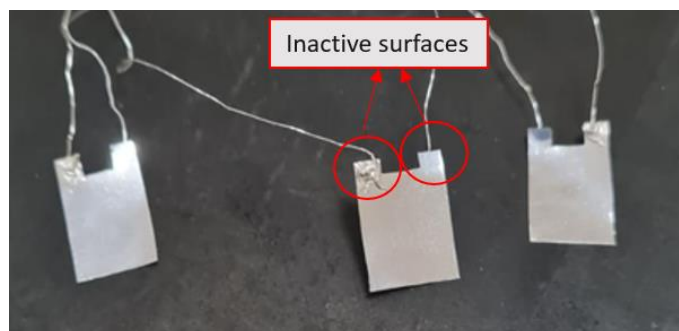


Figure 5.2 Sample Piezoelectric Patch Pictures

5.2. Experiment Setup

The excitation in the experimental run of the curved panel energy harvesting system was provided by TMS Modal Shop, K2007E01. Dewesoft Sirius DAQ card was used as the signal generator and data acquisition system. The accelerometer is Bruel & Kjaer 4507B004. All data were processed using the Dewesoft graphical user interface.

A fixture was produced in order to simulate the connection of the height of the panel produced in the experimental setup to the isolator which shown in Figure 5.3. The material is 3D printed and adhered to the floor to prevent movement during vibration. With the help of this product, the position of the shaker is fixed and a curved shape is formed at the desired radius of the panel.

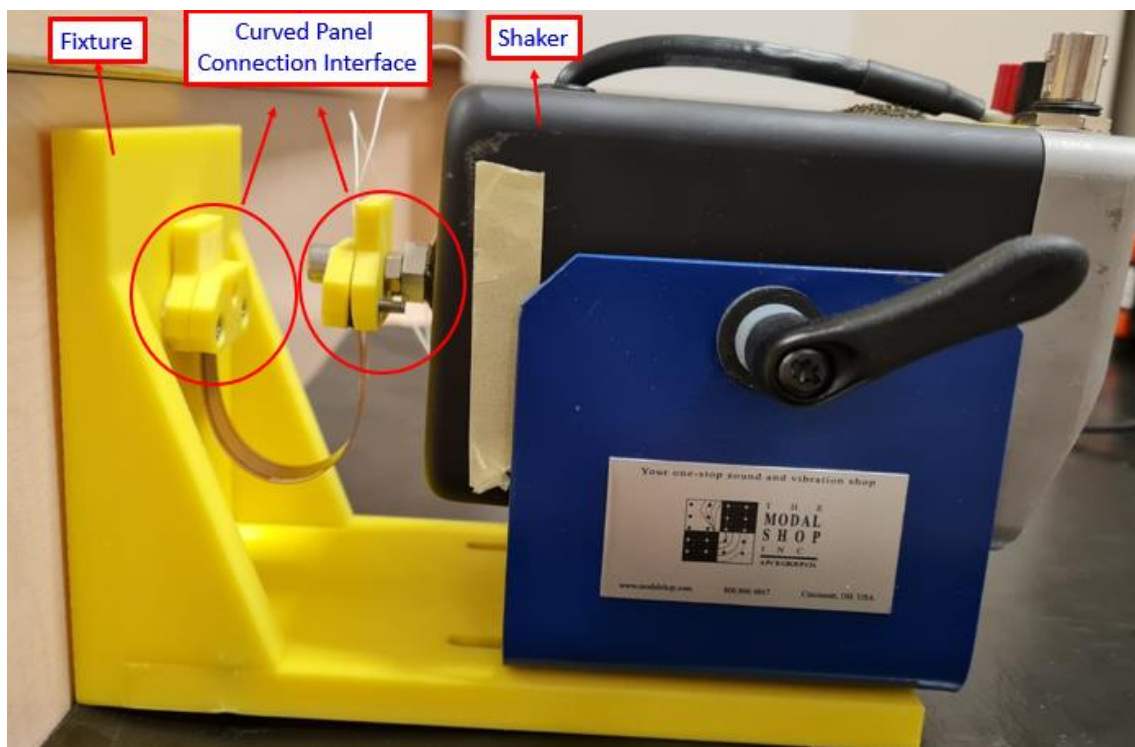


Figure 5.3 A Sample Picture Showing the Shaker, Fixture & Connection Interface

In order to connect the curved panel to the shaker and the fixture and to facilitate positioning, 4 connection pieces are designed as shown in the Figure 5.3. These parts are connected to the panel ends from the fixing surfaces and provide the connection interface for the shaker and the fixture. It also has a flat area for attaching the accelerometer to the area where excitation is given. Thus, the measurement is taken from the source of the acceleration. The other surface connected to the Fixture is considered to be fixed.

Within the scope of shaker and signal generator capabilities, the amplitude is 0.1 Voltage is set as input. The signal was applied as a logarithmic Sine sweep for 300 seconds. Logarithmic Sine sweep gives longer excitation at low frequencies and takes a short time at high frequencies. The applied signal is given in Figure 5.4 for 14 seconds. Data were collected up to 2000 Hz with 0.1526 resolution.

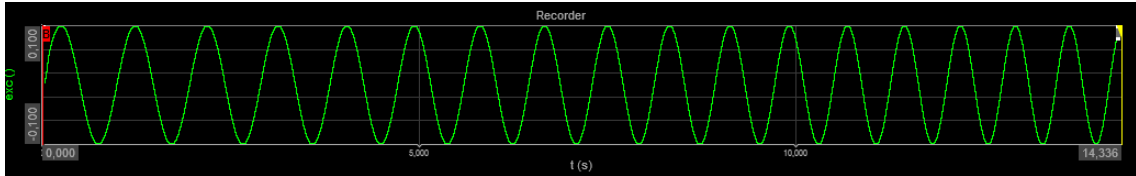


Figure 5.4 Excitation Signal of the Mechanical Shaker

Data processed using 67% overlap and hanning window as in isolator verification data.

When starting from a standing position, a spike occurs because the movement starts from the static state. Therefore, the data started to be collected after 1 Hz.

5.3. Experiment Results

In the EH experiment, the phases of the voltages to be generated from the piezoelectric patches cannot be known exactly. For this reason, the voltage data were taken from each patch separately without connecting the patches to each other. Thus, it is prevented that the patches with different phases are connected in the same direction and reduce the efficiency. At this stage, the experiment was repeated for each patch without creating an electrical connection between the patches.

Although the same test setup is used in each piezoelectric patch energy harvesting experiment, slight differences can be seen in the acceleration data as can be seen in the Figure 5.5. However, when viewed in the frequency domain, it is seen that the total gRMS values applied are close.

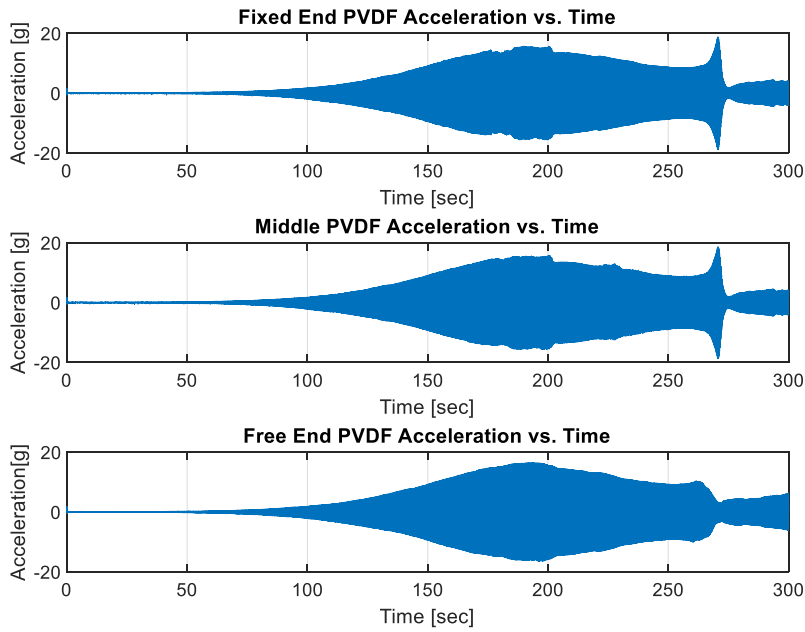


Figure 5.5 Acceleration-Time Data of PVDF Patches

The voltage time graphs obtained from the experiment are as in the Figure 5.6. When the graphs are examined, it is seen that the behaviors of the voltages obtained from the fixed end and the free end are similar, but the voltage obtained from the middle PVDF has a different behavior.

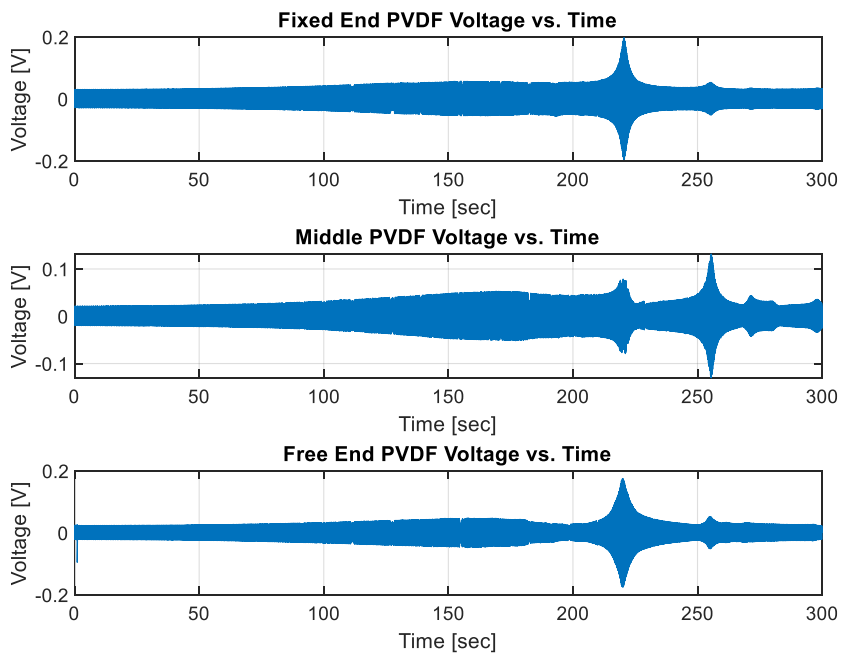


Figure 5.6 Voltage-Time Data of PVDF Patches

The graph in the Figure 5.7 was obtained when the voltage data was transformed from time domain to frequency domain. When the curved panel resonates during vibration, high voltage generation is obtained on the piezoelectric patches. Thus, by examining the Figure 5.7 the natural frequencies of the curved panel are found and also given in the Table 5.2

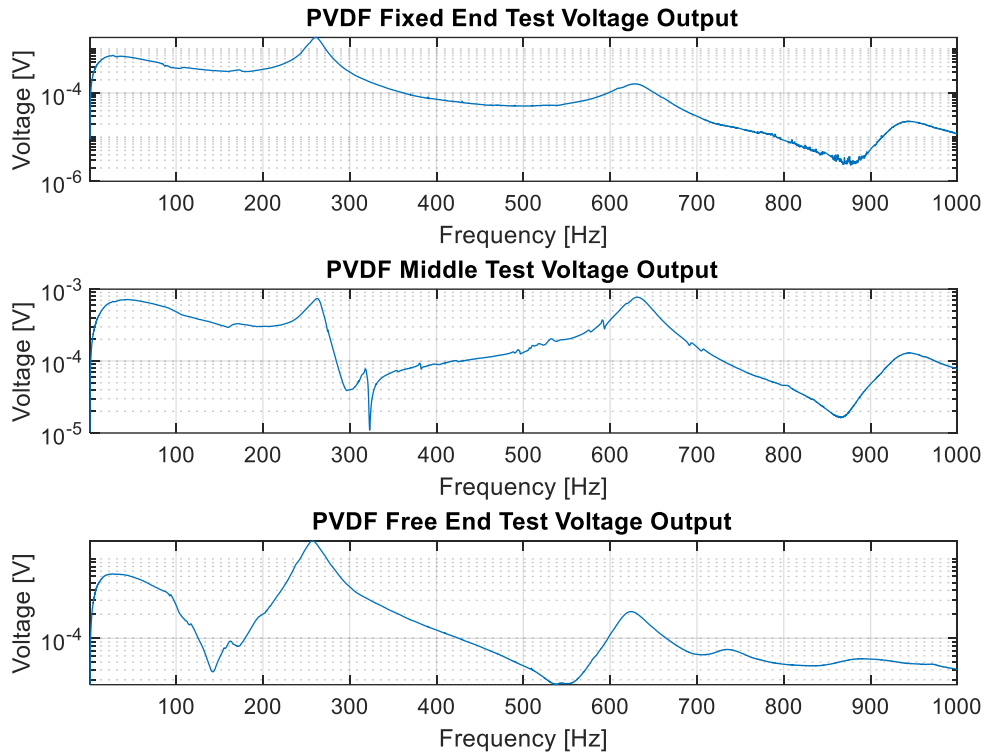


Figure 5.7 Voltage-Frequency Data of PVDF Patches

Table 5.2 First Two Modes of Curved Panel

Modes	Natural Frequency
1 st mode	260.8 Hz
2 nd mode	628.8 Hz

The graphs of acceleration data taken from the region where the shaker applied excitation in the experiment is shown in the Figure 5.8. The applied gRMS values are 5.78, 5.68, 5.60 for free end, middle and fixed end experiments, respectively.

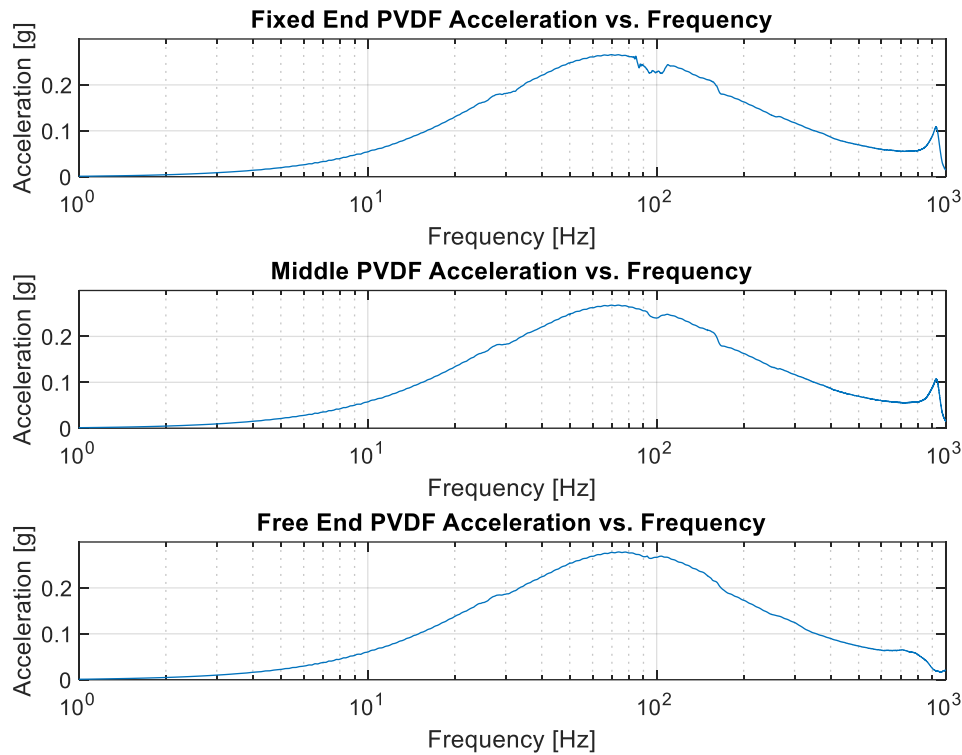


Figure 5.8 Applied Acceleration of PVDF Patches

In the verification of the FE model of the curved panel, the acceleration will be applied by taking the average value of the data given in the Figure 5.8.

5.4. Macro Fiber Composite (MFC) Experiment

The same energy harvesting study performed on the Curved Panel was performed using MFC. Thus, PVDF and MFC can be compared in terms of their efficiency.

MFC materials are soldered to copper cables from the solder surfaces on them. It is fixed on the fixture with the help of fixing parts. The active vibration length of the material is adjusted to be a semicircle on the WR isolator and connected.

Experiments were made for the voltage generated from 2 different widths of MFC materials. Thus, the role of width variation in energy production can also be examined. The MFC referred to as thick has an active width of 14mm, while the MFC referred to as thin has a width of 7 mm.

The voltage data measured in the time domain are given in the Figure 5.9 for both MFCs.

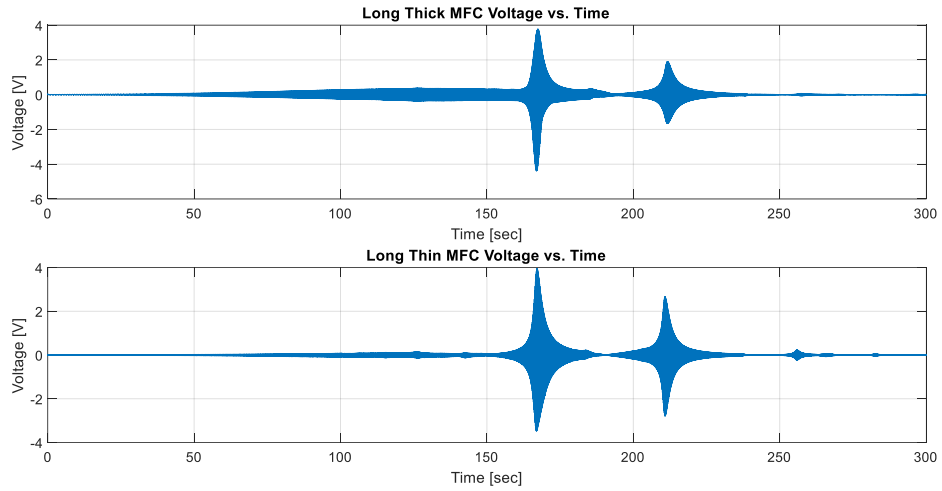


Figure 5.9 Voltage-Time Data of MFCs

In MFC experiments, 0.1V was applied as vibration input and the average of the data obtained as a result of the acceleration measurement was obtained and the graph in the Figure 5.10 was obtained.

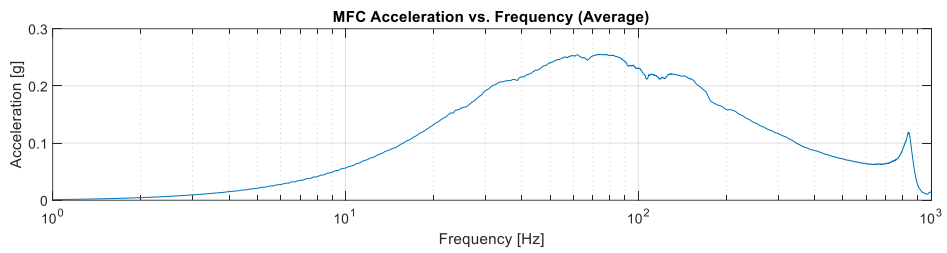


Figure 5.10 Average Acceleration-Frequency Data of MFC

The graph obtained by converting the measured voltage values to the frequency domain is shown in the Figure 5.11. At the same time, the frequencies with the high voltage values obtained in the graph are also given. Regions with high values were considered as the natural frequencies of the MFCs.

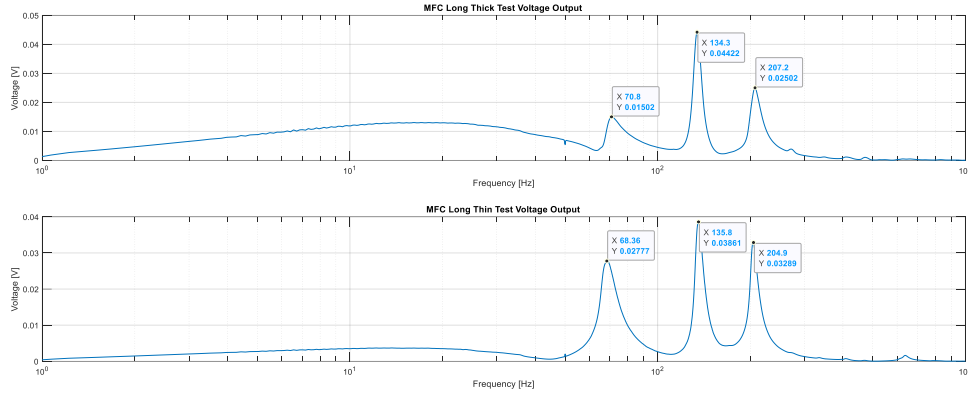


Figure 5.11 Voltage-Frequency Data of MFCs

Although the active voltage generation length of ready-made MFC materials is more than 60 mm, which is the length of the curved panel, their lengths are limited by being fixed during the experiment. In this way, only the effects of width are seen in natural frequency differences.

6. VERIFICATION OF FE MODEL

FE model of the curved panel and piezoelectric patches, which are the EH system used in the experiment, will be created. With this model to be created, the result of the FE analyzes should be close to the results obtained in the experiment. This verification has a critical importance in terms of sensitivity analyses to be made later in the study.

6.1. Boundary Conditions

The curved panel and piezoelectric patches FE model were created exactly the same as the dimensions used in the experiment.

In the experiment, one end of the curved panel is connected to the fixed wall, while the other end is connected to the shaker where the excitation is given. The end of the curved panel connected to the Shaker was accepted as free, and the end connected to the wall was considered fixed.

The free end is only released in the direction of the shaker movement and fixed in other axes. Fixed end is accepted as completely fixed. The excitation vibration acceleration measurements obtained from the experiment will be applied harmonic from the free end. Thus, the same case that occurred in the experiment will be simulated.

In the FE model, completely rigid flat extensions of 5 mm length were added to the fixed end and free end of the curved panel. Boundary conditions are applied to these surfaces.

The connection surfaces of curved panels of piezoelectric patches are treated as bonded. In this way, all the movement of the panel during vibration will be transmitted to the piezoelectric patches.

It is expected that the analyzes to be made under these boundary conditions and the data collected in the experiment will be close. However, this was not case due to the change in the material properties of the piezoelectric patches adhered to the curved panel. By making changes in the dielectric constants of the piezoelectric material, close values were reached and studies were continued in this way.

The FE model view of the boundary conditions of the established model is shown in the Figure 6.1.

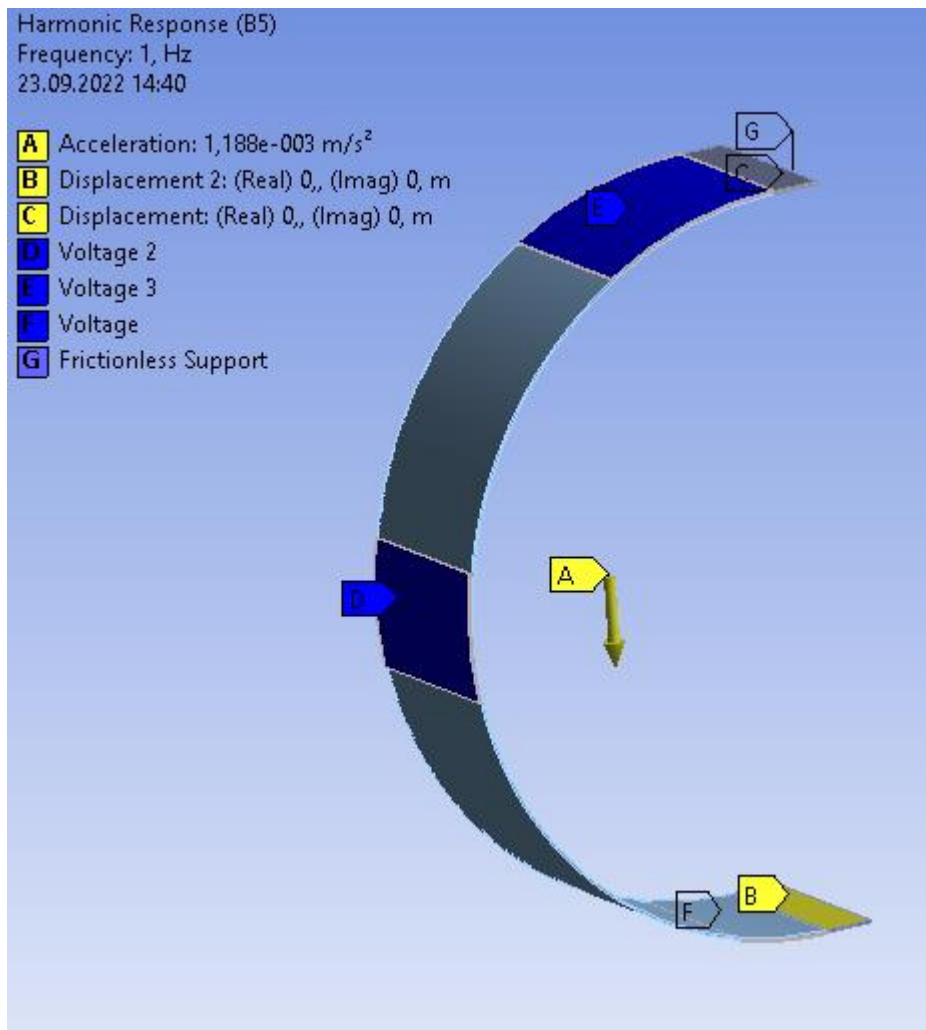


Figure 6.1 FE Model Boundary Conditions

6.2. Mesh Sensitivity Analysis

The voltage values obtained from the FE model depend substantially on the mesh structure. Since the model is a curved shape, it will be very challenging to mesh at high efficiency. In the formation of the mesh, the sweep method is used because the model is curved materials that continue at the same thickness. By combining this method with the body sizing method, the mesh is formed at the desired dimensions.

The obtained voltage data was converted to PSD, which is the unit of V^2/Hz to voltage RMS. RMS values were calculated from PSD data and compared.

Energy generation was controlled with meshes in different sizes. It is aimed to create high-accuracy energy in a short time by controlling the resolution times. The mesh size defined in body sizing is parametrically resolved. With the obtained data, the Table 6.1 was created.

Table 6.1 Mesh Sizing

Mesh Size [mm]	Voltage RMS [VRMS]	Elapsed Time [h]	1 st Mode [Hz]	2 nd Mode [Hz]	3 rd Mode [Hz]
1	7.740	0.39	258	625.47	1064.88
0.8	2.854	0.48	258.01	625.61	1063.84
0.5	0.684	0.74	257.91	625.11	1062.32
0.3	0.567	1.17	257.84	624.82	1061.34
0.1	0.499	4.94	257.76	624.49	1060.26

When the mesh sizes are examined, the voltage produced increases as the mesh size increases, but the shape of the curved panel cannot be fully achieved. The best quality curved shape is obtained as the mesh size is reduced. When the mesh size is reduced, the resolution time of the model increases significantly. Therefore, a choice will have to be made between the generated voltage and the resolution time.

When the 1 mm, 0.8 mm and 0.5 mm mesh sizes are examined, it is observed that there are large differences in energy production. For sensitivity study, the accuracy of the energy amount is more valuable than the analysis time. The 0.5 mm mesh size is reasonable among these three as it is close to the energy production of smaller mesh sizes and the resolution time does not increase dramatically.

When the voltage generation of 0.5 mm, 0.3 mm and 0.1 mm mesh sizes is examined, voltage outputs decrease by 17% between 0.5 mm and 0.3 mm mesh sizes, while resolution time increases by 58%. Between 0.3 mm and 0.1mm mesh sizes, while energy decreases by 12% in this comparison, time increases by 322%. Considering that sensitivity analysis will be made with many parameters as a result of these comparisons, it was decided to work with 0.3mm mesh size.

6.3. Verification Analysis

In this section, the voltage frequency graph and natural frequencies obtained in the curved panel EH experiment will be obtained by using Ansys modal analysis and harmonic analysis tools.

Ansys Harmonic analysis tool normally cannot analyze piezoelectric systems. It gains this ability with the help of the Piezo&MEMS module.

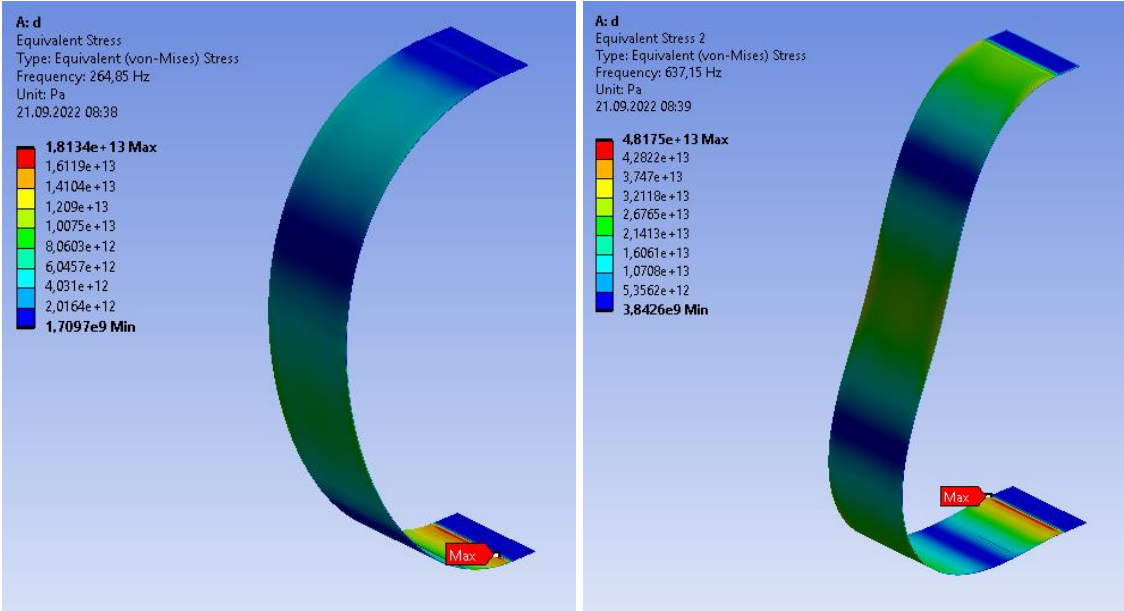
The modal analysis tool is only used to quickly obtain natural frequencies. Since the piezoelectric material also has its stiffness, it affects the natural frequencies of the curved panel while generating voltage. Therefore, piezoelectric patches should be defined as “Piezoelectric Body” in a modal analysis study.

In patches defined as piezoelectric body, voltage generation is provided by each node separately. As a result, the voltage value cannot be obtained collectively. It will be a huge problem to receive and analyze data from all nodes one by one. In order to prevent this, the nodes are connected to each other with the voltage coupling feature, which is also provided with the Piezo&MEMS module. Voltage coupling is used for all the nodes on the two wide faces of the piezoelectric materials.

Harmonic analysis study was solved with 1000 solution interval between 1-1000 Hz. One of the surfaces of the piezoelectric patches is defined as 0 V for ground effect.

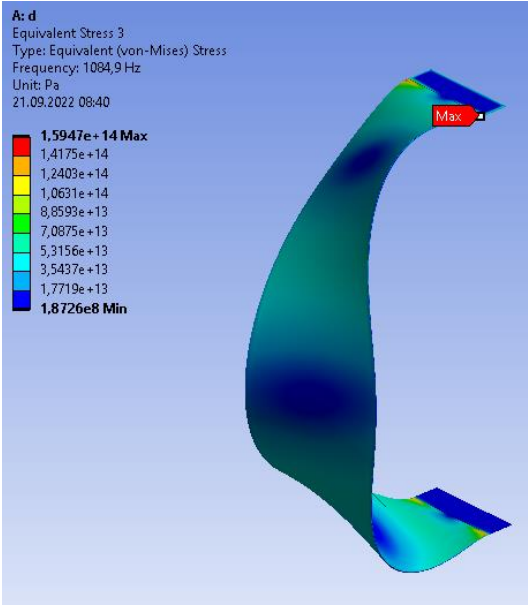
The acceleration value in the Figure 4.15 was used as the harmonic analysis input to the model.

As a result of the FE model analysis created, the mode shapes of natural frequencies are shown in the Figure 6.2. Since the deformation is high in the first 3 mode, the voltages generated are high.



(a)

(b)



(c)

Figure 6.2 Mode Shapes of FE Model: 1st mode (a), 2nd mode (b), 3rd mode (c)

The first 3 modes of the curved panel EHS are given in the Table 6.2.

Table 6.2 FE Model Natural Frequencies

1st Mode	265.85 Hz
2nd Mode	637.15 Hz
3rd Mode	1084.9 Hz

Voltage-frequency graphs of harmonic analysis and test results are given in the Figure 6.3.

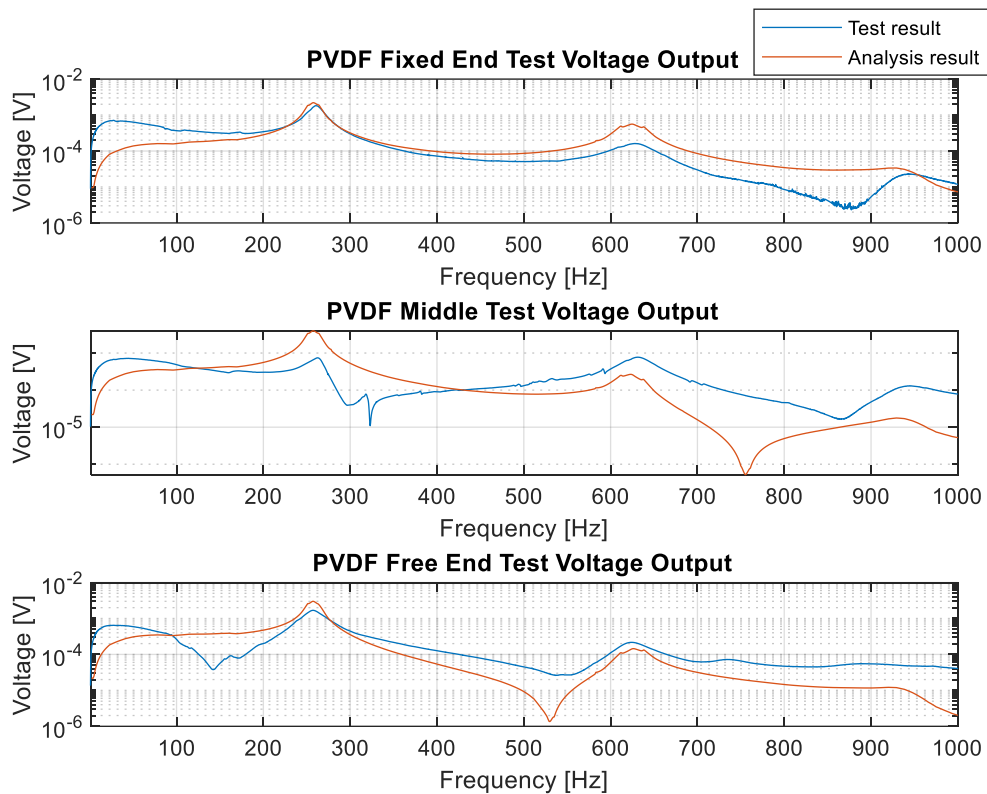


Figure 6.3 FEM Analysis Result vs. Test Result

Figure 6.3 when examined, it is seen that the voltage generated in the experiment and the voltage trends obtained as a result of the analysis are close to each other. For comparison, the Hanning window and resolution used during the measurement were considered in converting the measurement data to PSD and RMS. The voltage and voltage difference percentages are given in the Table 6.3 for the test and analysis results.

Table 6.3 Analysis vs. Test Result

	Test Results [VRMS]	FEM Analysis Result [VRMS]	VRMS Difference [%]
Fixed End Patch	0.2232	0.2061	7.7
Middle Patch	0.0658	0.0716	-8.8
Free End Patch	0.1918	0.1829	4.6

The difference of the experiment and FEM analysis results is occurred due to the production tolerances of the test parts and assembly differences of the patches used in the experiment.

The graph of the relative acceleration in the verification study of the isolator which excited with $0.006 \text{ g}^2/\text{Hz}$ white noise and the acceleration values used in the verification of the curved panel are given in

Figure 6.4. It is observed that the vibration profile used in isolator verification is lower than the vibration profile in curved panel verification. When the total applied energies are compared, energy is harvested by applying 5.25 gRMS power in curved panel verification, while 3.43 gRMS power will be applied in isolator verification. Based on this, the voltage obtained from the curved panel verification experiment is expected to be higher. However, when the curved panel is connected to the isolator, there is a change in the amount of energy to be generated due to the configuration.

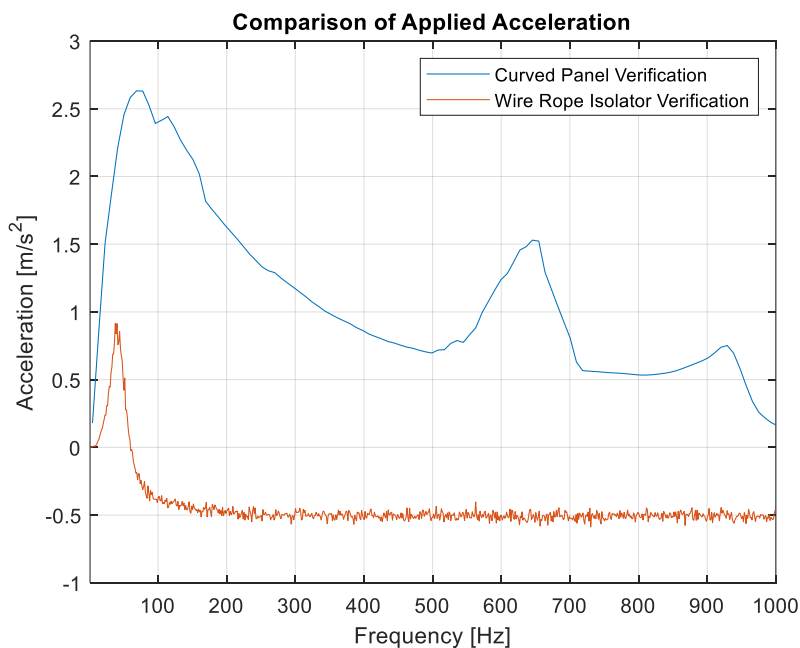


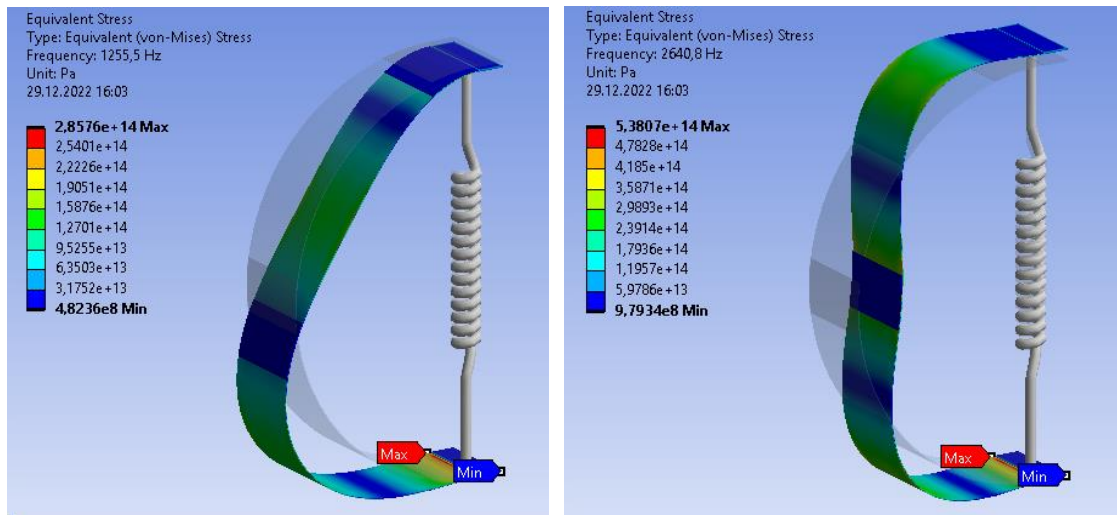
Figure 6.4 Comparison of Applied Accelerations

7. ENERGY HARVESTING SENSITIVITY ANALYSES

In this section, the curved panel energy harvesting system will be optimized with the FE model verified in the curved panel section to be excited by using the vibration data obtained from the vibration isolator section in the Ansys MAPDL harmonic analysis tool. Thus, the voltage graph that will occur when the EH system is connected to the isolator will be obtained in the frequency domain.

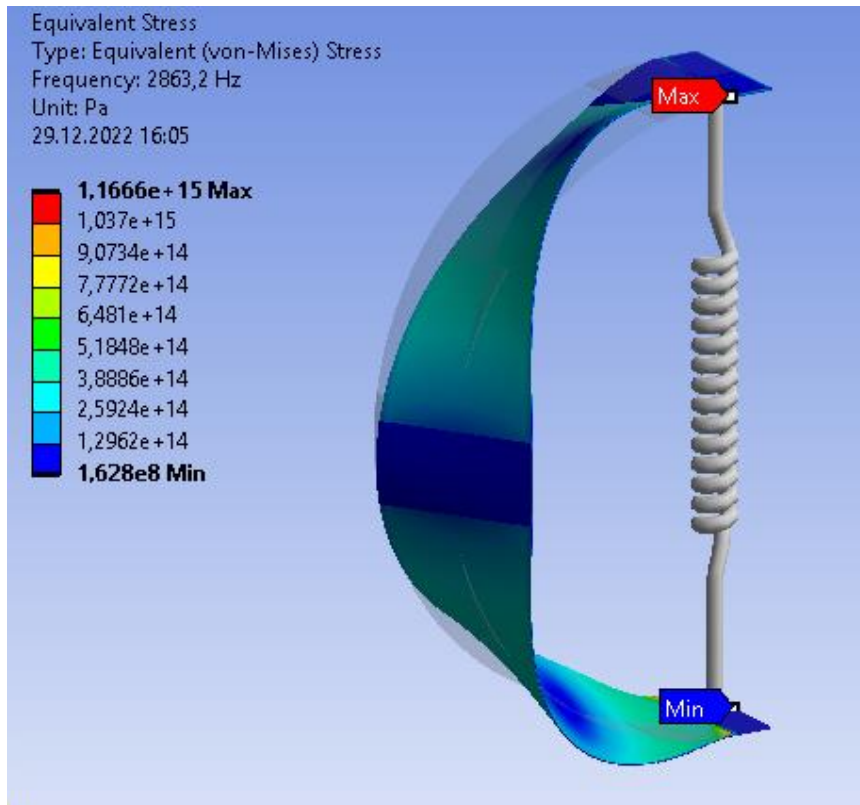
The relative acceleration of $0.006 \text{ g}^2/\text{Hz}$ PSD input given in the Figure 4.15 was applied to the verified FE model from the free end.

As a result, the graphic in the Figure 6.3 has been reached. This graph is accepted as the voltage-frequency graph that will be generated when the curved panel is attached to the mass isolator system. Since the curved panel will be connected to the isolator system, a spring is defined between the two ends of the curved panel. The spring will represent the behavior and stiffness of the isolator. Under these conditions, while the mode shapes of the curved panels did not change, there were great changes in natural frequencies. Mode shapes are given in the Figure 7.1.



a)

b)



c)

Figure 7.1 Mode Shapes of Isolated FE Model:

1st mode (a), 2nd mode (b), 3rd mode (c)

The natural frequencies of isolator mounted curved panel are given in the Table 7.1.

Table 7.1 Isolated FE Model Natural Frequencies

1st Mode	1255.5 Hz
2nd Mode	2640.8 Hz
3rd Mode	2863.2 Hz

In order to increase the efficiency and the generated voltage of the CP EHS connected to the isolator system, sensitivity analyses will be made by changing dimensions.

First of all, it is tried to reach the values at which the highest voltage is obtained by changing the angle covered by the piezoelectric patches on the CP. Patches with the

highest energy generation or energy density will be selected for the surfaces to which they are attached. Then, by changing the widths of the CP and patches, the effect of the curved panels on the stiffness of the isolator system and its role in the voltage generation were examined. After the high voltage obtained width is found, the studies will be started in which the thickness of the piezoelectric patches is changed. In this study, varying voltage generation and energy efficiency differences will be examined when the piezoelectric patch thicknesses are changed. Changing these parameters will cause changes in the natural frequencies and behavior of the system. As a result of the analyzes to be made, the changes in the system behaviors will be examined.

7.1. Angle Sensitivity Analysis

In this sensitivity study, it is aimed to create high energy output by changing the angle of the piezoelectric patches on the curved panel. Positive and negative charges that occur simultaneously due to mode shape on a single piezoelectric patch reduce the total energy output. Therefore, by changing the areas covered by the piezoelectric patches, the effect of compression and tension acting on the patch at the same time is reduced the efficiency. In the region where one of the stresses is more dominant, a higher voltage output will occur. Thus, efficiency will be increased.

The angles covered by the patch have been increased by 5° and started from 15° . The patch length is 4.97 mm when the 15° angle is covered. Considering the piezoelectric patch production, sensitivity work was started with this minimum angle. There is a possibility that the patches to be produced at angles above 50° may touch each other during the experiment. For this reason, studies were continued up to an angle of 50° .

Figure 7.2 was obtained when the acceleration data in Figure 4.15, taken from the isolator verification, were applied to the established model.

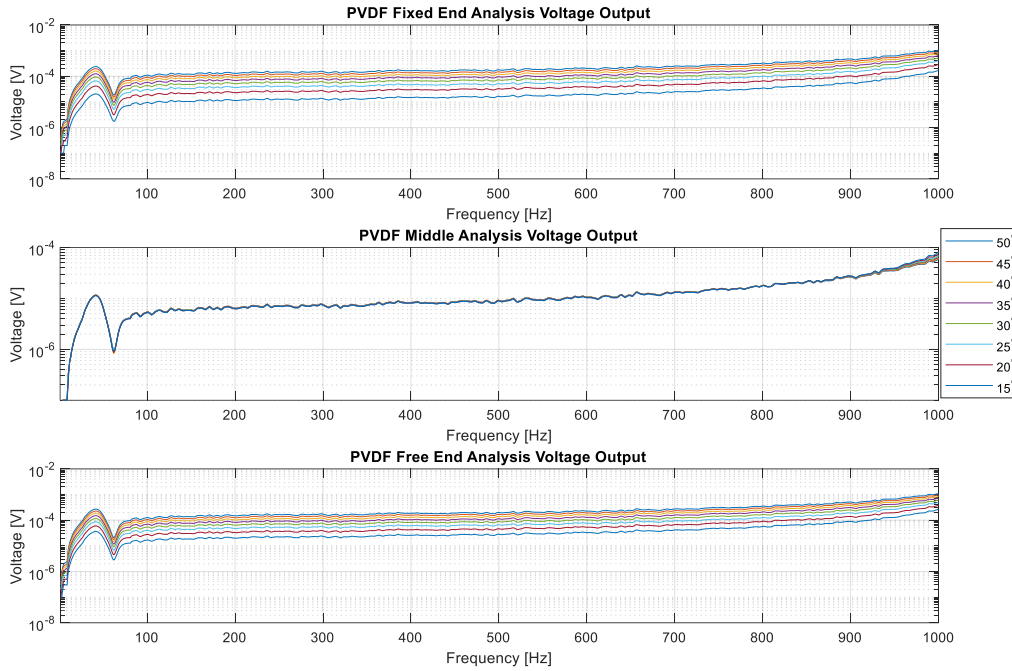


Figure 7.2 Piezoelectric Patch Covered Angle Sensitivity Graph

When Figure 7.2 is examined, it is noteworthy that the natural frequencies of the curved panel are not seen in this frequency band. Due to the natural frequency of the isolator system, it is seen that high acceleration has a magnificent effect on the voltage generation. The effect of the reflection of the stiffness value of the isolator system on the curved panel has clearly emerged in this context.

The energy values generated for each analysis are given in the Table 7.2 and Figure 7.3. The behavior curves of the results of the parametric study done in Figure 7.3 are also seen. When the amount of energy generated is examined, the highest energy for the fixed and free end patches are provided with a 50° patch, while the energy increases as the covered angle increases. In the middle patch, the highest energy production was obtained at 50° patch. Besides, it is observed that there is no significant change in the amount of energy generated as the angle is changed. Close energy productions have occurred in all middle patch models.

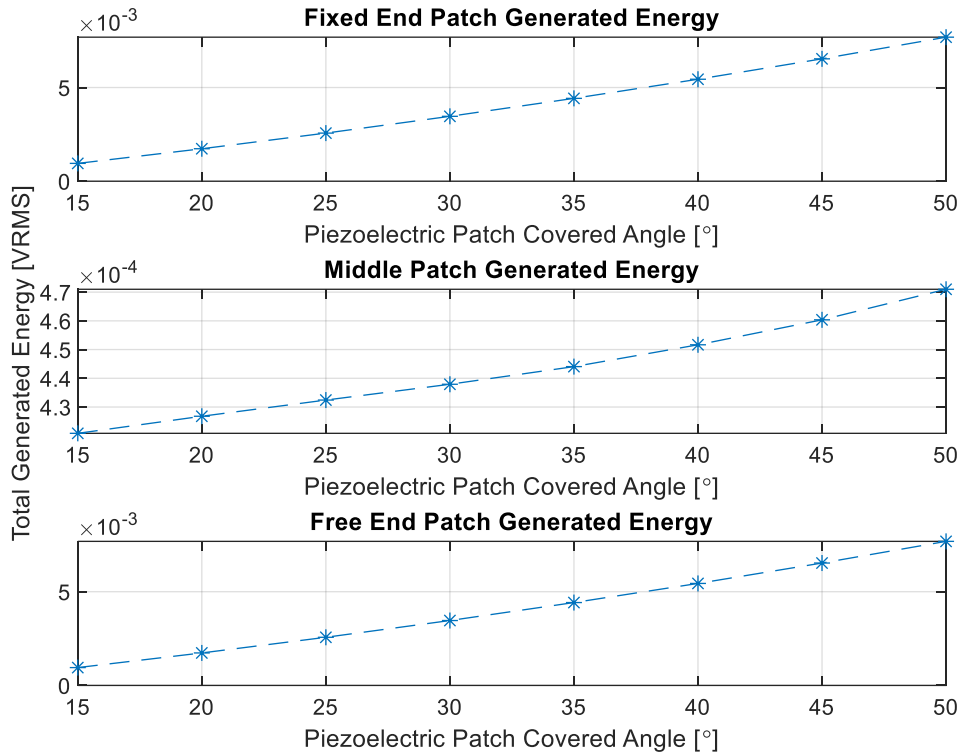


Figure 7.3 Piezoelectric Patch Covered Angle Voltage Trend

Table 7.2 Piezoelectric Patch Covered Angle Voltage Data

Patch Covered Angle	Fixed End Patch [VRMS]	Middle Patch [VRMS]	Free End Patch [VRMS]
15°	0.0015	0.00042	0.0010
20°	0.0023	0.00043	0.0017
25°	0.0032	0.00043	0.0026
30°	0.0041	0.00044	0.0035
35°	0.0051	0.00044	0.0044
40°	0.0061	0.00045	0.0054
45°	0.0072	0.00045	0.0065
50°	0.0083	0.00047	0.0077

The ratio of the generated energies to the volumes of the piezoelectric materials is defined as the energy density. While the behavior graphics of the energy densities are given in the Figure 7.4, the energy density data are given in the Table 7.3.

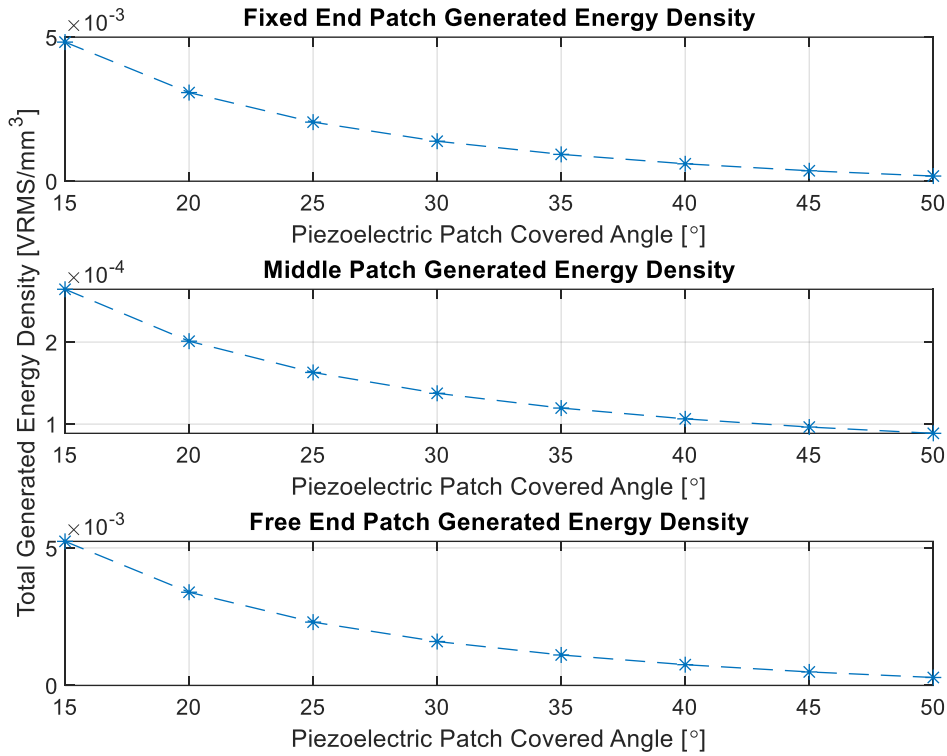


Figure 7.4 Piezoelectric Patch Covered Angle VRMS Density Trend

Table 7.3 Piezoelectric Patch Covered Angle VRMS Density Data

Patch Covered Angle	Fixed End Patch [VRMS/mm ³]	Middle Patch [VRMS/mm ³]	Free End Patch [VRMS/mm ³]
15°	0.0052	0.00026	0.0048
20°	0.0034	0.00020	0.0031
25°	0.0023	0.00016	0.0021
30°	0.0016	0.00014	0.0014
35°	0.0011	0.00012	0.0009
40°	0.0008	0.00011	0.0006
45°	0.0005	0.00010	0.0004
50°	0.0003	0.00009	0.0002

When the data obtained are examined, it is seen that at the all patches the energy efficiency decreases as the piezoelectric patch covered angle increases. According to this result, sensitivity analysis will continue with some of selection. While the energy production is aimed to be high, the efficiency should not decrease. However, due to the inverse proportion of these, some choices will be made.

When we examine all the results, the highest energy generation and energy generation density occurs in 15° free end patch. Therefore, this is the most convenient patch to attach on the free end.

The closest energy generation of fixed end patch to free end patch was realized in 30° patch. Considering the importance of energy production, a 30° covered patch was chosen by compromising efficiency while choosing a fixed end patch.

Looking at the middle patch, it is seen that there is no big difference in energy production when the covered angle is changed. Since there may be big changes in other sensitivity analyses in this patch, which has almost no change in this study, a 20° covered patch has been chosen so that the effects can be observed easily.

7.2. Width Sensitivity Analysis

In this section, voltage output will be examined by changing the width of the piezoelectric material, with chosen covered angle in angle sensitivity analysis section. Angle sensitivity analysis was carried out with 8 mm wide curved panel. The width sensitivity analysis will be started from 6 mm so that the production of the piezoelectric patch is not difficult. There is no upper limit to the piezoelectric patch width. However, since the curved panel has stiffness, the stiffness increases as its thickness increases. Considering that the curved panel is connected to the isolator system, the stiffness value of the curved panel will have an effect on the system. For this reason, a preliminary study of the stiffness values of the curved panel will be made and the widest curved panel and piezoelectric patch that can be used will be found.

The stiffness values of the curved panel when it was in the shape of a semicircle were found. Since the isolator stiffness value is nonlinear, it was taken from the manufacturer's catalog. In the calculation, panel stiffness values up to 15 mm width were found. Since the stiffness behavior of the curved panels is nonlinear, the highest stiffness values are included in the calculation. When these values were compared with the lowest stiffness value of the WR isolator, Table 7.4 was obtained.

Table 7.4 Curved Panel-WRI Stiffness Ratio

Curved Panel Width [mm]	6	7	8	9	10	11	12	13	14	15
Stiffness Percentage [%]	7.13	8.34	9.55	10.76	11.97	13.15	14.36	15.57	16.78	17.97

While assigning the maximum width of the curved panel, care was taken to ensure that the stiffness value was less than 15% of the minimum WR isolator stiffness. Accordingly, the sensitivity work will be executed by increasing the width by 1 mm from 6 mm to 12 mm.

In the verified energy harvesting model, the width value was changed parametrically. The voltage frequency data obtained as a result of the study are given in Figure 7.5.

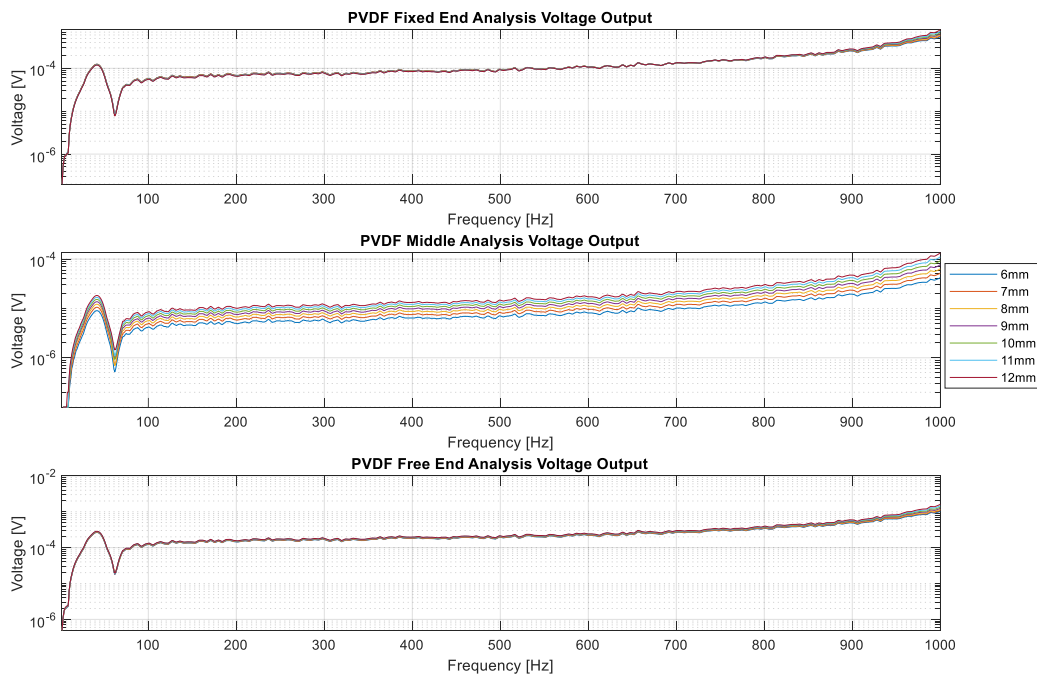


Figure 7.5 Piezoelectric Patch Width Sensitivity Analysis Graph

When the created voltage frequency graph is examined, it is observed that there is no change in natural frequencies and the voltages generated are close to each other for fixed and free end patches. On the other hand, it is clearly seen that the energy production increases as the width increases in the middle patch.

The voltage values generated by each patch are collected according to phase angles and they created the total energy. Total energy density was obtained by dividing the volumes of the piezoelectric patches. The data collected for comparison can be made in the Table 7.5.

Table 7.5 Piezoelectric Patch Width Energy Density Data

Curved Panel Width [mm]	Voltage RMS [VRMS]	Voltage RMS Density [VRMS/mm ³]
6	0.0124	0.0024
7	0.0128	0.0021
8	0.0132	0.0019
9	0.0137	0.0018
10	0.0143	0.0017
11	0.0149	0.0016
12	0.0156	0.0015

Considering the data of the Table 7.5, it is seen that the highest energy generation is provided by the material with a width of 12 mm. However, as the material width increases, the energy density decreases. In addition, the panel width will increase the effect of the isolator system to be mounted. Therefore, studies will continue with 9mm, which is the middle value of both energy generation and energy density.

To visualize the overall trend of total energy and energy density graphics are given in Figure 7.6 and Figure 7.7, respectively.

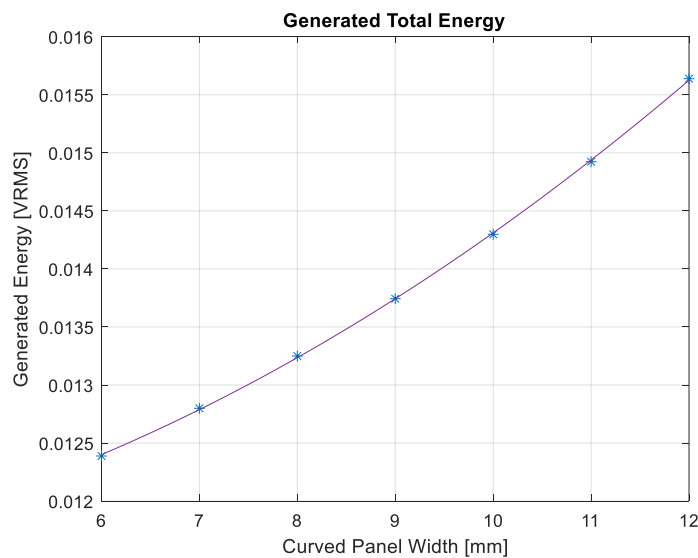


Figure 7.6 Piezoelectric Patch Width Voltage RMS Trend

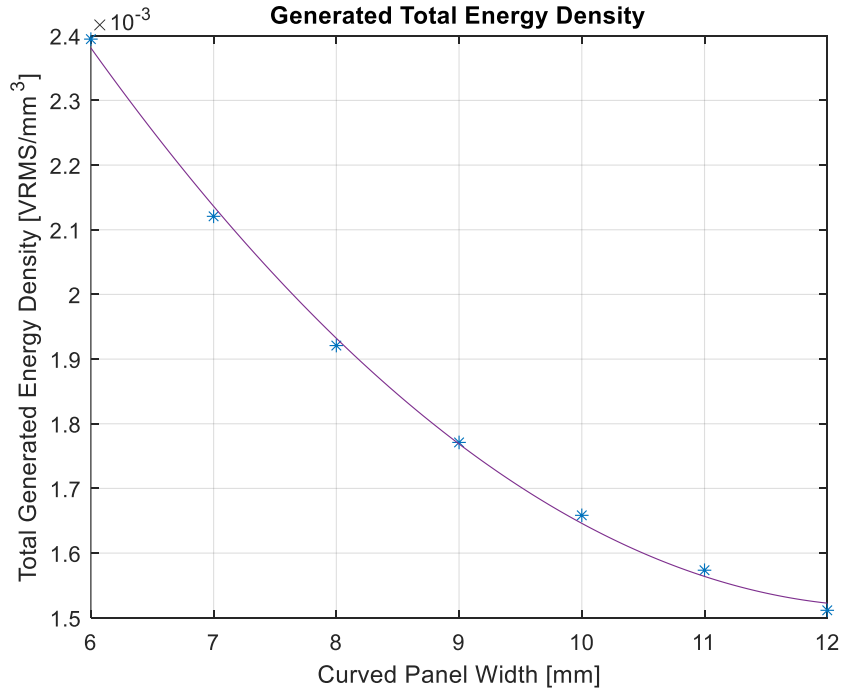


Figure 7.7 Piezoelectric Patch Width Voltage RMS Density Trend

7.3. Thickness Sensitivity Analysis

In this section, where the thickness of the piezoelectric patches will be changed, the effect of the patch on the natural frequencies of the system and the changes in energy production will be examined. Material thickness is preferred as 40 microns, 80 microns and 110 microns. These thicknesses of the piezoelectric polymer can be found in the market easily.

When the relative acceleration for $0.006 \text{ g}^2/\text{Hz}$ input taken from the isolator verification section is applied, the voltage frequency graph on all patches is given in Figure 7.8.

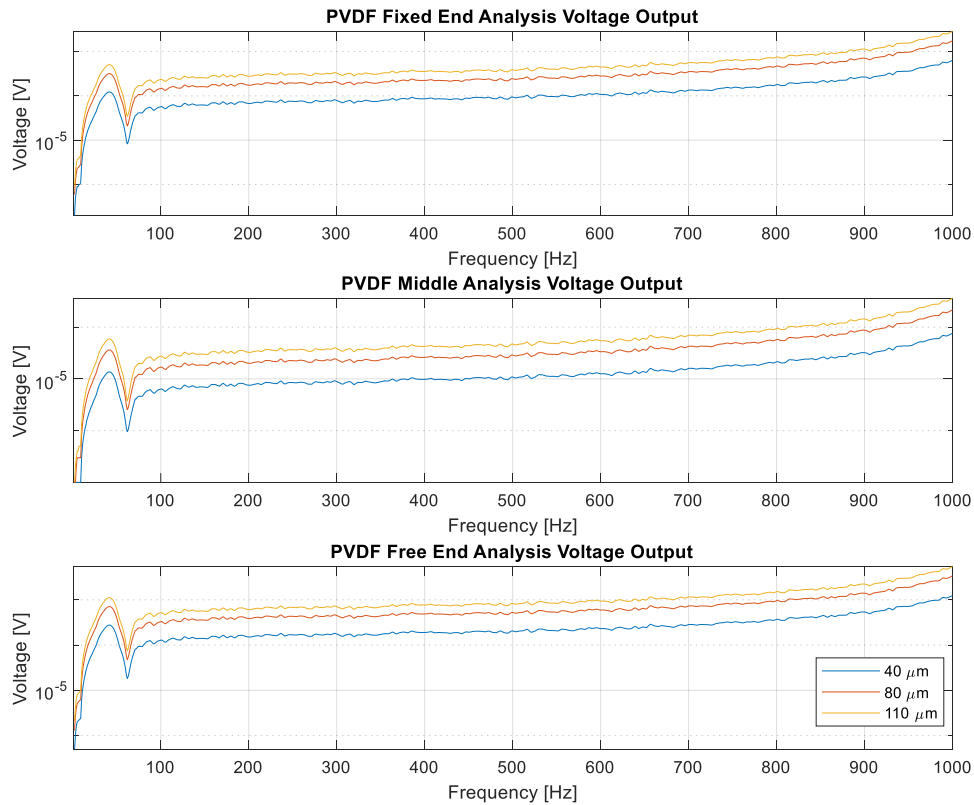


Figure 7.8 Piezoelectric Patch Thickness Sensitivity Analysis Graph

When the change of natural frequencies is examined, the difference is not observed in the isolator excited mode and the modes of the curved panel in this frequency band.

Total voltage-frequency values and total energy density values collected according to their phases from all piezoelectric patches are given in Table 7.6.

Table 7.6 Piezoelectric Patch Thickness Energy Density Data

Piezoelectric Patch Thickness [μm]	Voltage RMS [VRMS]	Voltage RMS Density [VRMS/ mm^3]
40	0.0137	0.0018
80	0.0363	0.0023
110	0.0580	0.0027

Looking at the results of the FE analysis, it is seen that the patches with 110 μm thickness stand out among the total energy values obtained. Likewise, when evaluated in terms of

total energy densities, it is obvious that the efficiency is higher. Based on these results, when piezoelectric patches with 110 μm thickness and 9 mm width are placed by covering free end 15°, middle 20°, fixed end 30° angle, energy harvesting is achieved with the highest energy output and efficiency.

7.4. Selected Patches Verification

In this section, the curved panel and piezoelectric patches produced in selected sizes as a result of the FE analyzes were mounted to the isolator system and energy was harvested. The obtained results were compared with the FE analysis results.

The patches that were decided to be used after the sensitivity studies were produced as in the CP verification experiment. The 9 mm curved panel is obtained as flat by laser cutting from sheet metal. The region where the vibration source is accepted as fixed, and the region where the mass is attached is accepted as free. The patches produced in this context were attached to the curved panel as in the verification study. The produced panel was first taped up to the isolator. Then, by screwing the isolators to the fixture and the mass, they are tightened between them and completely fixed. The experimental setup is shown in the Figure 7.9.

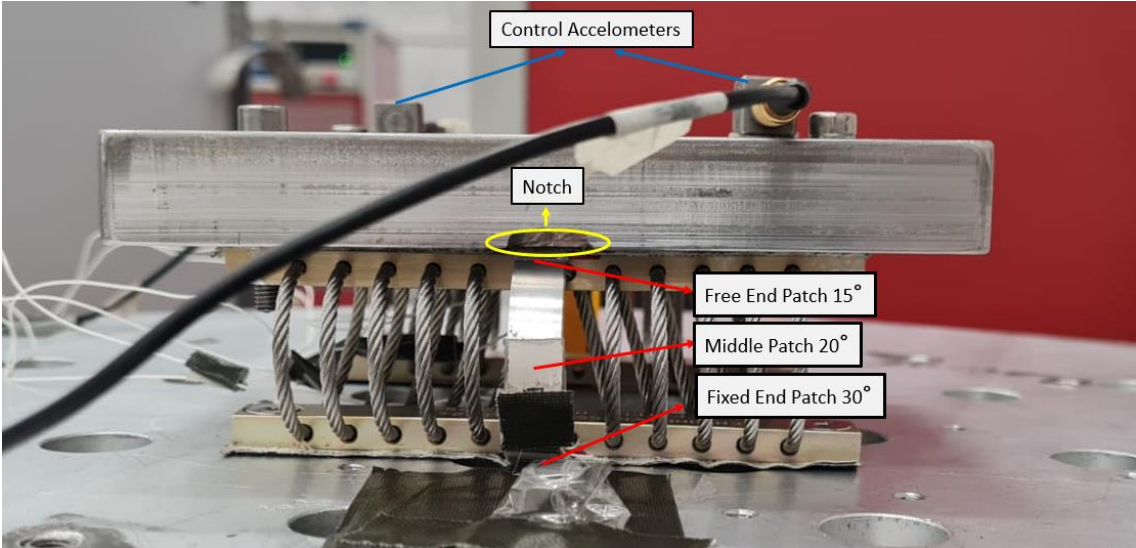


Figure 7.9 Final Experiment Setup

In order not to restrict the vertical movement of the CP during the experiment, notches were made on the fixture and the mass in the areas where the EHS will be mounted. The notch on the mass is shown in the Figure 7.9.

Finite element analysis work has been performed for $0.006 \text{ g}^2/\text{Hz}$ white noise base excitation in the previous sections. For this reason, this vibration profile was applied from the base in the final result verification. The voltage-time graphs obtained during the experiment are given in the Figure 7.10.

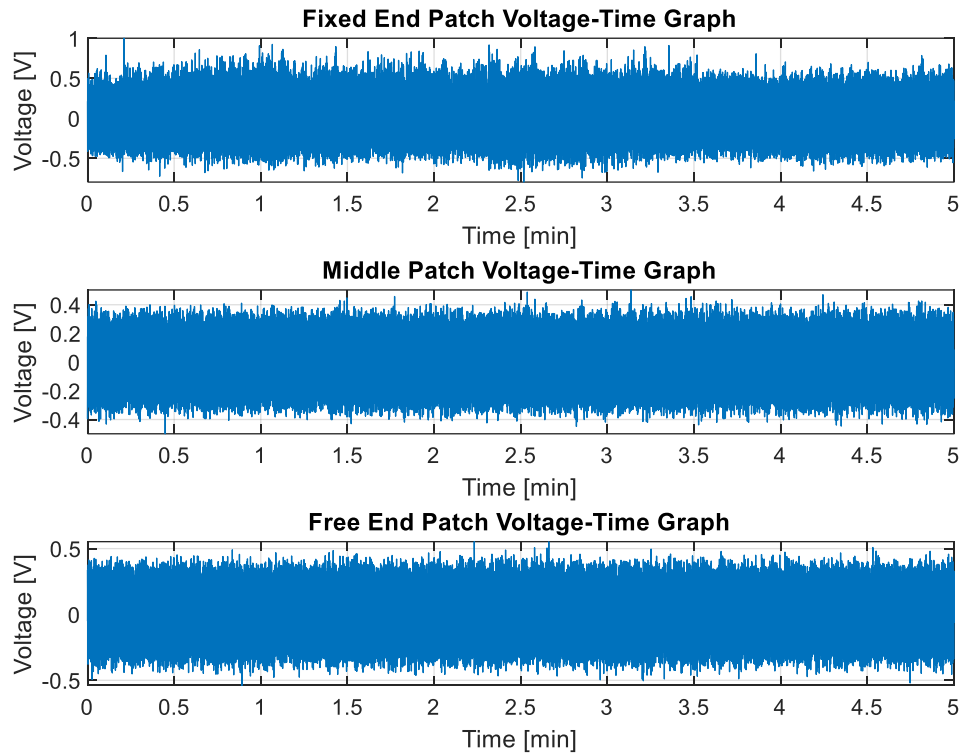


Figure 7.10 Voltage-Time Graph of Final Experiment

When the voltage-time graphs are examined, the highest voltage generation is obtained from the fixed end patch, which has the largest surface area, while the lowest voltage generation occurs in the middle patch, as seen in the FE analyses.

Dewesoft software was used when switching from time domain to frequency domain and the filters were applied the same as in the curved panel verification part. The voltage-frequency graph created as a result of the experiment is given in the Figure 7.11.

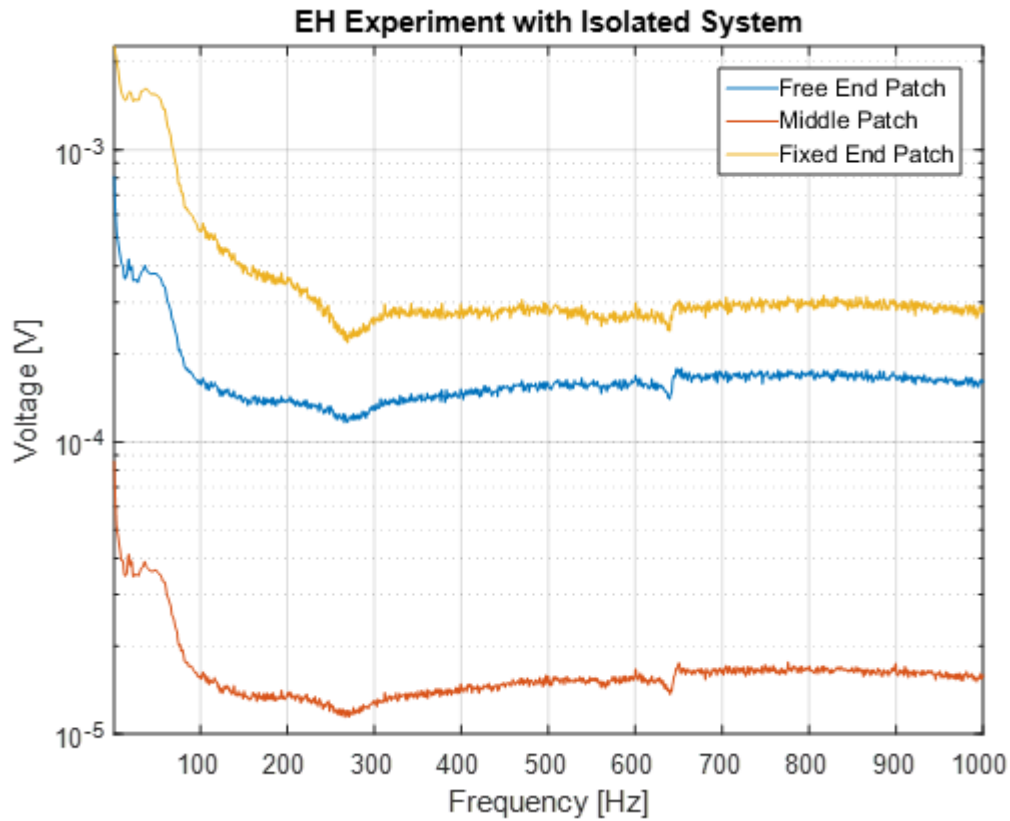


Figure 7.11 Voltage-Frequency Graph of Final Experiment

When the Figure 7.11 is examined, it is seen that the highest energy output is obtained by the fixed patch. After the fixed end patch, which has the largest area, high energy output was observed from the free end patch, which has the smallest surface area, as can be predicted from the results of the FE analyzes. The lowest energy output occurred in the middle patch. As expected from the results of the analysis, high voltage generation occurred near 40 Hz, originating from the first natural frequency of the isolator system.

The comparison of the voltage frequency graph obtained from the FE analysis and the graphic obtained as a result of the experiment is given in the Figure 7.12.

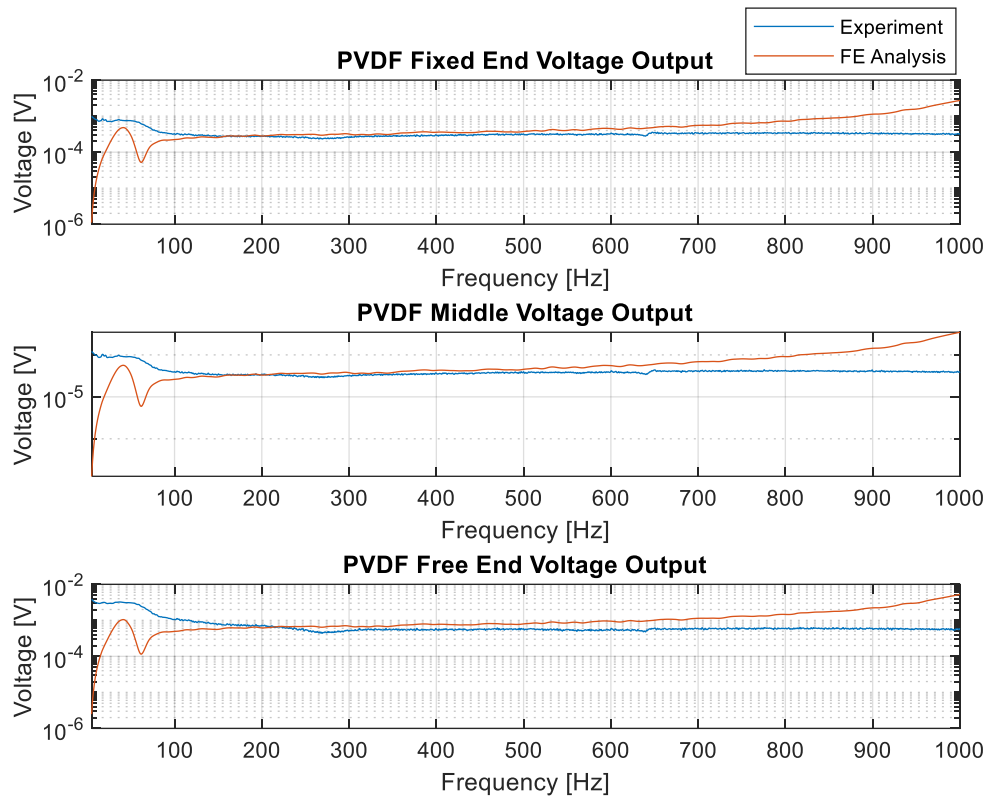


Figure 7.12 Comparison of FE Analysis and Final Experiment Results

When the Figure 7.12 is examined, although the graphic behaviors show similarities in some regions, the differences draw attention. One of the main reasons for these differences is the non-linearity of damping of WRI, and the other is the frequencies at which the relative motion between the fixture and the mass is 0 or close to 0. Although the damping ratio is defined linearly to the FE model, it creates differences in the test and analysis results due to the non-linear behavior of the isolator.

In the regions where the relative motion is close to 0 (where the transmissibility is close to 1), it is accepted that the curved panel does not affect acceleration in the FE model. Due to these regions voltage drops occur in the analysis results. However, at these frequencies, where there is no relative motion and both ends of the CP act as fixed, the vibration profile coming from the base affects the panel. This provides the voltage generation and not be seen voltage drops in the test results.

Table 7.7 FE Analysis and Final Experiment Generated Energy Data

	Fixed End Patch	Middle Patch	Free End Patch	Total
FE Analysis Generated Voltage RMS [VRMS]	0.0375	0.0016	0.0190	0.0580
Experiment Generated Voltage RMS [VRMS]	0.0928	0.0041	0.0406	0.1374
Difference (After 30 Hz) [%]	15.17	19.89	18.68	17.91

Comparison of the generated energies is given in the Table 7.7. The energy generated in the experiment is about 20% more than the energy obtained from the analysis. Due to the large differences between the data obtained up to 30 Hz, the difference percentages are included for frequencies after 30 Hz. The highest energy difference occurred in the middle patch, which generated the least energy. The lowest energy difference occurred in the fixed end patch, where the highest energy generated zone.

8. CASE STUDIES

This section includes the experiments and analysis studies in addition to the FE analysis and experiment studies. Energy was harvested by applying real vibration profiles. Methods have been tried to increase energy efficiency. Compared with PVDF using different energy harvesting material (MFC).

8.1. Helicopter Vibration Profile

The behavior of the EHS, which is produced and mounted on the vibration table, in different vibration profiles and the amount of energy they will generate will be examined. a military helicopter vibration profile which is 6.06 gRMS, was applied to this system and the obtained voltage-time graph is given in the Figure 8.1.

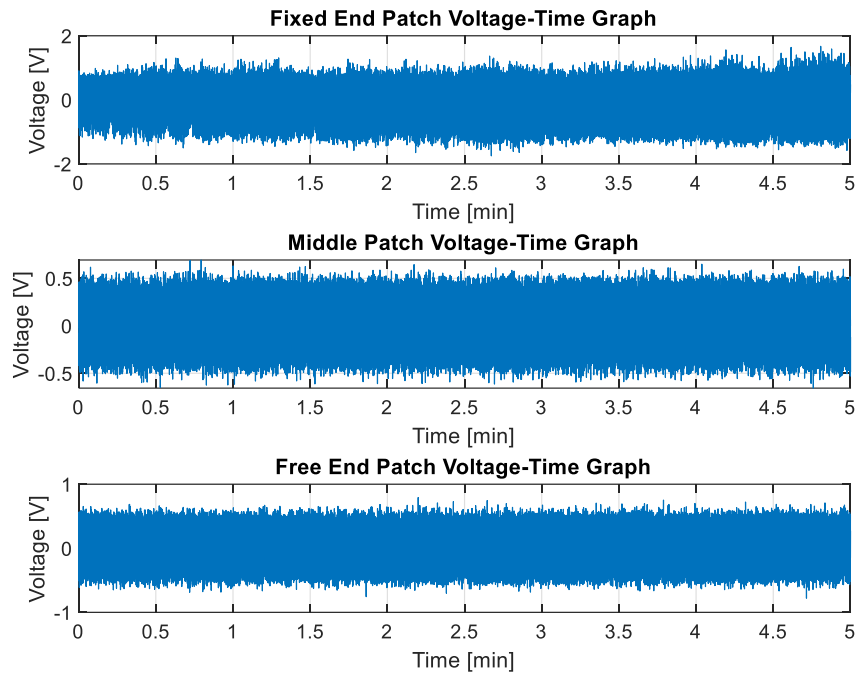


Figure 8.1 Voltage-Time Graph of Helicopter Vibration Profile

As can be seen from the Figure 8.1, there is a continuous voltage generation in the system. While the highest energy output is seen on the fixed end patch, the lowest energy generation occurs in the middle patch. Voltage graph obtained when transforming from time domain to frequency domain is given in the Figure 8.2.

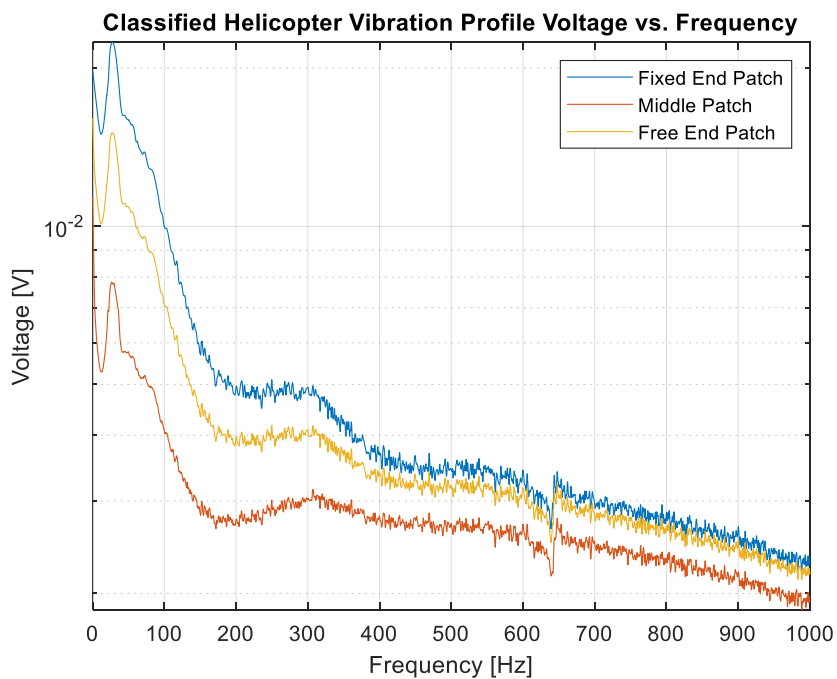


Figure 8.2 Classified Helicopter Vibration Profile Energy Harvesting

The voltage ratios produced are close to the results of white noise, but higher due to the graphic vibration profile. When white noise vibration is applied with 3.46 gRMS input, the total energy obtained is 0.1374 VRMS, while the energy collected with 6.06 gRMS helicopter vibration is 0.2942 VRMS.

8.2. Gun Fire Vibration Profile

A generic vibration profile, which occurs when firing a gun mounted on military vehicles and combined with vehicle motion, was applied to the test setup. The voltage-time graph obtained as a result of this profile, which has different peaks and drops at different frequencies, is given in the Figure 8.3.

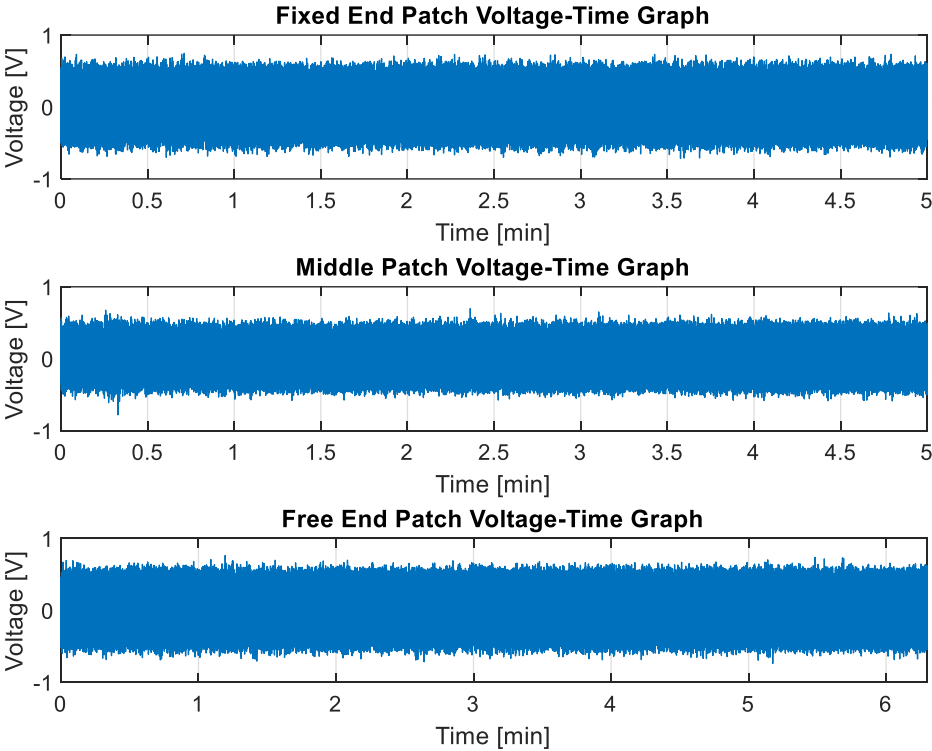


Figure 8.3 Voltage-Time Graph of Gun Fire Vibration Profile

Although all generated voltage amounts seem close to each other for this vibration profile, the middle patch generated lower energy. For the all-patches voltage-frequency graphs are shown in the Figure 8.4.

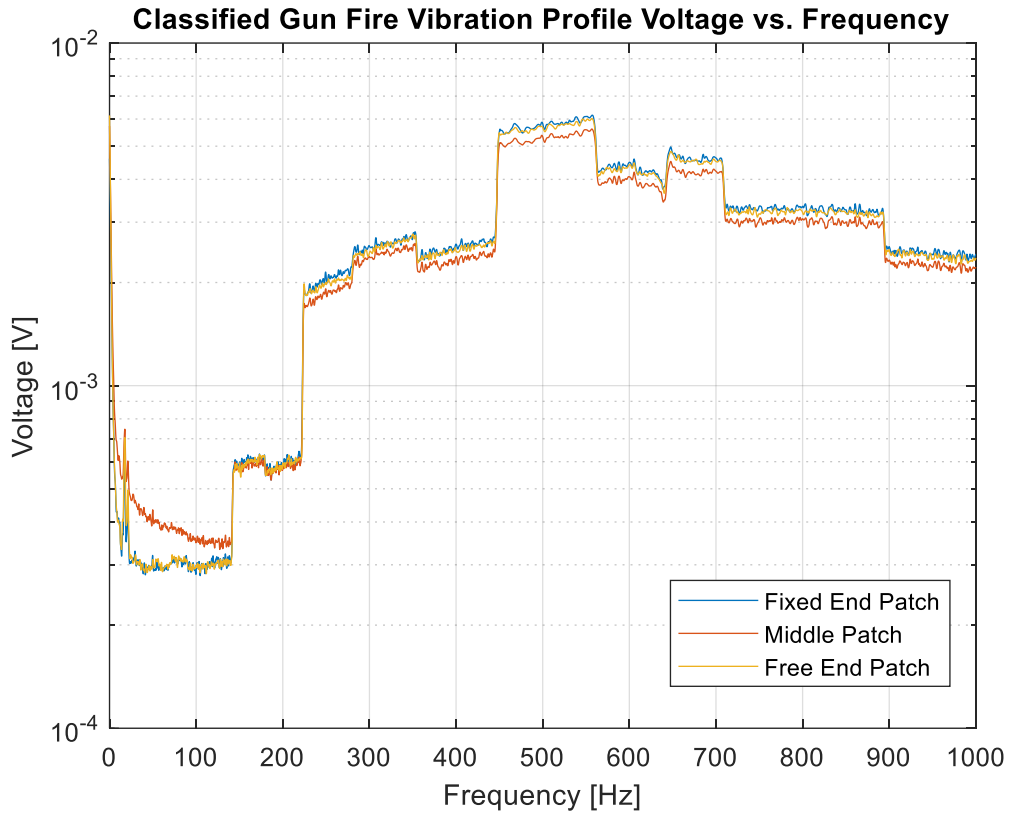


Figure 8.4 Classified Gun Fire Vibration Profile Energy Harvesting

When Figure 8.4 is examined, it is observed that the voltage outputs of all patches have a close profile, while at low frequencies the middle patch generates higher voltage than the others. At high frequencies, the contribution of middle patch to voltage generation is lower than other patches.

While the total PSD value of the applied gun fire vibration profile is 6.71 gRMS, the energy generated is 0.2708 VRMS.

8.3. MFC

During the CP verification study, energy harvesting was also carried out with MFC panels and the results were evaluated. Long thin MFC (85mm x 7mm), which has the highest power density, is connected to the isolator in a full semicircle and vibration profiles applied to the curved panel are applied. The excess remaining length of this material, which has more than the required length, is completely fixed on the fixture, preventing

its effect on energy production. The time graph of the voltage generated in the experiment is shown in the Figure 8.5.

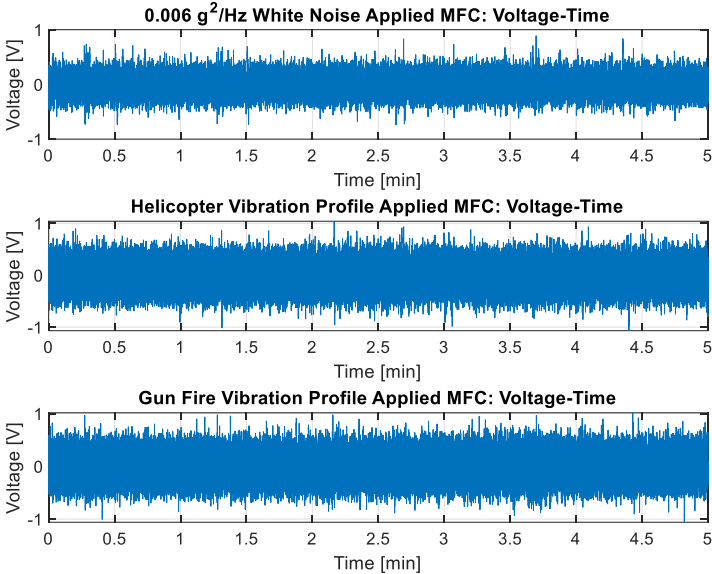


Figure 8.5 Voltage-Time Graph of Different Vibration Profile

When the time graphs are examined, it is seen that the voltage generated in the white noise profile is less than the others. For the other two profiles, the voltage outputs are close to each other. The voltage graphs in the frequency domain are given in the Figure 8.6.

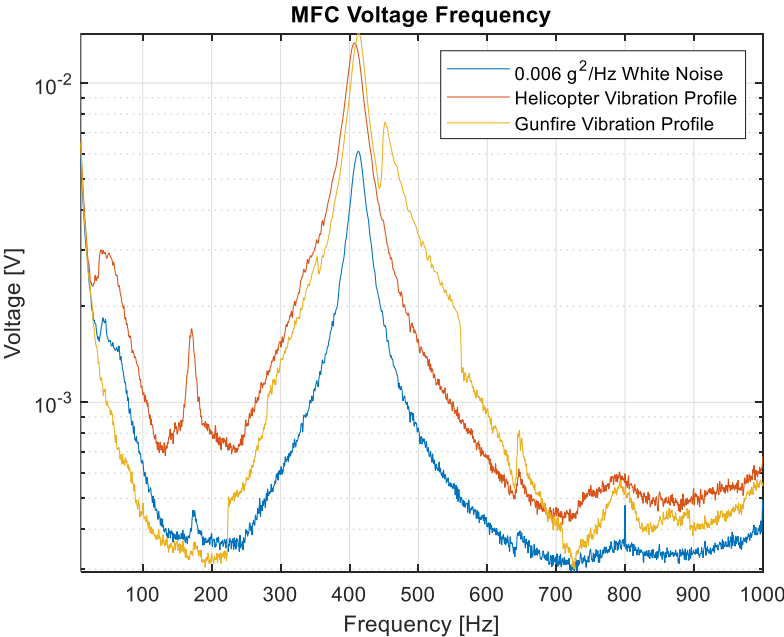


Figure 8.6 Voltage-Frequency Graph of Different Vibration Profile

Looking at figure 8.6, the first thing that stands out is that the helicopter vibration profile excites the first mode of the MFC more, increasing the energy production at 163 Hz. At 414 Hz, the highest energy harvest was occurred for all profiles.

The total amount of energy generated is collected in the Table 8.1.

Table 8.1 MFC Experiment Generated Energy

Applied Vibration Profile	Voltage RMS [VRMS]	Applied gRMS
White Noise	0.0858	3.46
Helicopter	0.1527	6.06
Gun Fire	0.1469	6.71

Since the helicopter vibration profile is better in providing more movement of the first mode of the MFC, the highest energy output is obtained here, although the applied vibration energy is lower than Gun Fire vibration profile. When the amount of energy generated is examined, it is seen that it is lower than the amount produced in the Section 5. At the same time, PVDF materials, which have a much lower active area than themselves, generate much higher energy thanks to their placement in the right areas of the curved panel.

8.4. CP Mode Sensitivity Analysis

In the analysis study, when the CP is attached to the isolator system, it is seen that the natural frequency of the CP is not the natural frequency in the frequency band of interest. For this reason, a custom material was created by changing the steel material of the CP. By reducing the elastic modulus of the material, it is ensured that the 1st and 2nd modes of the CP are below 1000 Hz. The voltage frequency graph of the new FE model created is given in the Figure 8.7.

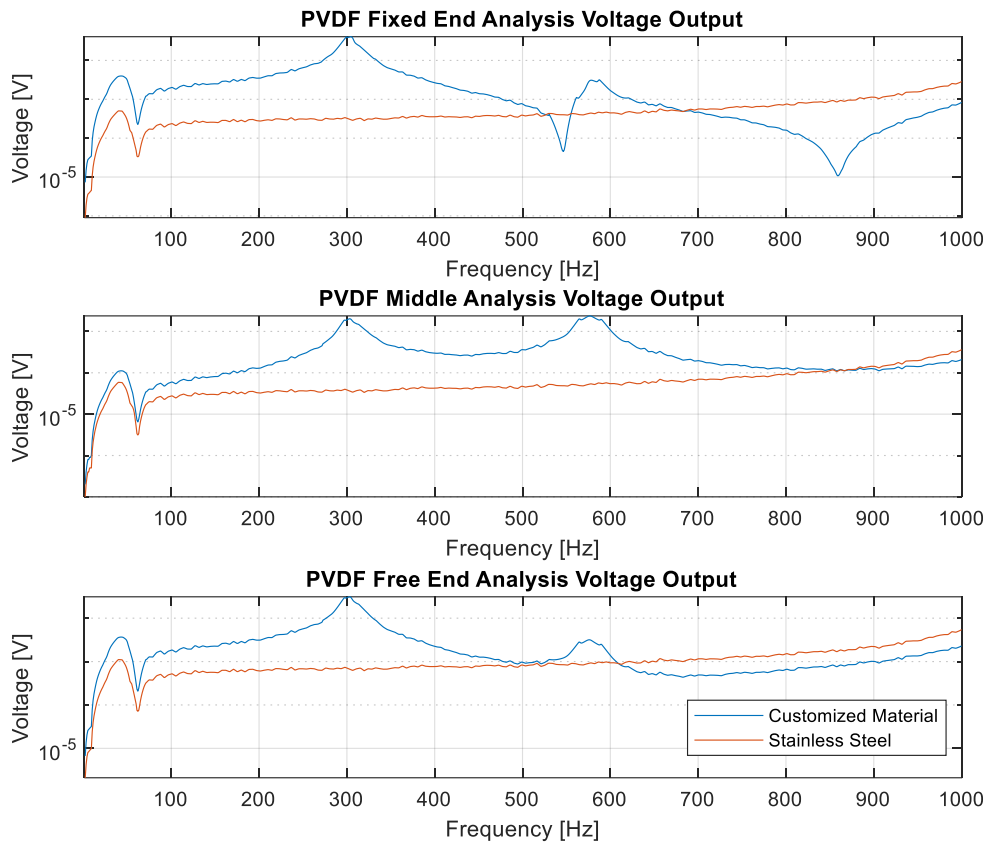


Figure 8.7 Customized Material CP vs Steel CP Energy Harvesting

When the Figure 8.7 is examined, since the custom material is more deformable, it generates a higher voltage even than the high acceleration caused by the natural frequency of the isolator system. It realizes much higher voltage production with the effect of its own natural frequencies.

Energy generations of custom material CP and steel CP are compared in the Table 8.2.

Table 8.2 Customized Material CP vs Steel CP

Curved Panel Material	Voltage RMS [VRMS]	Voltage RMS Density [VRMS/mm ³]
Customized	0.3186	0.0149
Steel	0.0580	0.0027

According to data from Table 8.2 , customized material CP generates 4.5 times more energy than steel CP. This high energy, provided with the same piezoelectric patches, increases the energy density (efficiency) at the same rate.

9. DISCUSSIONS AND CONCLUSION

Within the scope of this thesis, an energy harvesting system has been developed to meet the energy needs of sensors that can be placed on a passively isolated military air platform. The energy harvesting system consists of piezoelectric patches placed on the curved panel to be connected between the base of the isolator and the mass. First of all, different amplitude white noises were applied from base to determine the characteristics of the isolator system. The behavior of the non-linear isolator system has been examined and verified. The most difficult problem in this section was that even the slightest pre-stress that the isolator system may be exposed while connecting, affects the results. In order to prevent this, all of the screws connected at each stage were gradually torqued. Thus, it is prevented that one side gets stuck and constricts the other sides and affects the test results. Another point to note is that the torque values are equal and a torque meter was used during assembly.

The excitation applied from the base of the isolators acts on the EHS to be placed in between with the movement of the mass. Curved panel is exposed to relative motion between these two regions. This relative motion ensures that the amplification that occurs during the natural frequency of the isolator system also excites the EHS extra. Thus, the standard base excitation applied increases even more, affects the energy harvest and increases the efficiency. Increasing the natural frequency number of the isolated system will also increase the vibration intensity that will affect the EHS, thus, energy production will increase.

In the next step, work has been done to verify the curved panel, which will form the skeleton of energy harvesting. Piezoelectric patches were adhered to certain areas on the curved panel with the information obtained from the preliminary studies. In the preliminary analysis, the high stressed regions of the curved panel exposed to vibration were selected. One end of the panel was fixed to the designed experimental setup, and the other end was connected to the shaker and a sine sweep excitation was applied. With the voltage outputs on PVDF materials, the behavior of the curved surface on which an accelerometer cannot be placed has been observed. This means that data can be obtained by attaching PVDF patches in cases where measurements are required on inclined surfaces.

The wiring is attached to the piezoelectric patches with a silver-containing adhesive. However, when the adhesive cures, it becomes rigid and will negatively affect energy production/efficiency. For this reason, protrusions are placed on the patches for the areas where the adhesive will be applied. Care was taken not to touch the conductive area on the back surface of the adhesive and not to cause a short circuit. Thus, the problem of decrease in efficiency has been resolved.

The biggest problem experienced while creating the FE model was that the energy generation properties of PVDF materials changed when adhered to the curved surface. Numerous attempts were made on the material properties to match the FE analysis results with the data obtained in the CP verification study. For this reason, it was worked with a single diameter curved panel.

In the energy harvesting study, the CP connected to the isolator system has a natural frequency of up to 1000 Hz, which is of great importance in terms of efficiency. However, in the energy harvesting study conducted here, the mode of the CP did not have a great effect on energy generation.

After the sensitivity studies, patches and panels were produced in the dimensions decided and mounted on the isolator system. The energy output obtained as a result of the FE analyzes was compared with the energy output observed in the experiment. There were differences between the results. The main reason for these differences is that the acceleration applied in the FE analysis is only the relative acceleration between the mass and the base. Because at the frequency where the relative motion is 0, the CP is base excited. Although there was no movement between the fixed and free ends, the material vibrated due to its own weight and played a role in energy production. Since this part was not taken into account in the analysis study, the energy production remained low at low frequencies and at the frequency after $\sqrt{2}$ times the natural frequency of the isolator system. This causes the difference to appear large when the total energy output is calculated. Another reason why the results are different is that the neutral axis also changes when bent due to the increase in the thickness of the piezoelectric patch. Therefore, the piezoelectric material properties for which the FE model was initially verified did not fully meet the properties of the piezoelectric material used in the experiment.

In the case study, the behavior of the EHS under different vibration profiles was investigated. Increases in energy generation were observed with increasing the vibration profile. However, the high vibration profile in regions without natural frequencies had less effect on energy generation. For this reason, higher voltage output can be obtained if the natural frequency of the CP is in the frequency region where the vibration profile is high.

One of the ways to reduce the natural frequency of the curved panel is to change its material. By varying the material of the panel as in section 8.4, natural frequencies in the frequency band of interest can be obtained. Thus, energy production increases exponentially. Another method is to reduce the thickness of the CP. If it gets thinner, its hardness will decrease and its natural frequency will decrease. With another approach, serious reductions in natural frequency can be achieved by making topology optimization on the CP. If the vibration profile of the platform it will be installed on is known, higher energy harvesting will be achieved with the EHS to be produced in accordance with the needs.

In the first study, in line with the studies made with MFC materials, much higher energy outputs were observed during the sine sweep compared to the PVDF material. However, due to the semi-circular shape of the material, the positive and negative charges neutralize each other due to the simultaneous compression and tension effect on its body during movement. For this reason, all the energy generated is lost before being harvested and the efficiency is greatly reduced. In the last experiment, more than two times more energy was generated with the PVDF piezoelectric patch, which has a much lower surface area than itself.

High voltage generation was observed in the curved panel verification study in the middle patch. When the curved panel is connected to the isolator, there is a significant reduction in voltage generation. The negative effect of the increased stiffness between the two ends of the curved panel on the energy production in the middle patch was observed.

REFERENCES

- [1] E.I. Rivin, Vibration isolation of precision equipment, *Precision Engineering* 17(1) (1995) 41-56.
- [2] R. Ibrahim, Recent advances in nonlinear passive vibration isolators, *Journal of sound and vibration* 314(3-5) (2008) 371-452.
- [3] K. Kowalczyk, H.-J. Karkosch, P.M. Marienfeld, F. Svaricek, Rapid control prototyping of active vibration control systems in automotive applications, 2006 IEEE conference on computer aided control system design, 2006 IEEE international conference on control applications, 2006 IEEE international symposium on intelligent control, IEEE, 2006, pp. 2677-2682.
- [4] D. Karnopp, *Active and semi-active vibration isolation*, (1995).
- [5] A. Mallik, V. Kher, M. Puri, H. Hatwal, On the modelling of non-linear elastomeric vibration isolators, *Journal of Sound and Vibration* 219(2) (1999) 239-253.
- [6] P. Balaji, M. Rahman, L. Moussa, H.H. Lau, Wire rope isolators for vibration isolation of equipment and structures—A review, *IOP conference series: materials science and engineering*, IOP Publishing, 2015, p. 012001.
- [7] S. Chalasani, J.M. Conrad, A survey of energy harvesting sources for embedded systems, *IEEE SoutheastCon 2008*, IEEE, 2008, pp. 442-447.
- [8] Y.K. Tan, S.K. Panda, Self-autonomous wireless sensor nodes with wind energy harvesting for remote sensing of wind-driven wildfire spread, *IEEE Transactions on Instrumentation and Measurement* 60(4) (2011) 1367-1377.
- [9] D. Hao, L. Qi, A.M. Tairab, A. Ahmed, A. Azam, D. Luo, Y. Pan, Z. Zhang, J. Yan, Solar energy harvesting technologies for PV self-powered applications: A comprehensive review, *Renewable Energy* (2022).
- [10] C. Bowen, H. Kim, P. Weaver, S. Dunn, Piezoelectric and ferroelectric materials and structures for energy harvesting applications, *Energy & Environmental Science* 7(1) (2014) 25-44.
- [11] S. Boisseau, G. Despesse, B.A. Seddik, Electrostatic conversion for vibration energy harvesting, *Small-scale energy harvesting* 5 (2012).
- [12] A.P. Pérez, *Proyecto Fin de Carrera Ingeniería Eléctrica*.
- [13] B. Yang, C. Lee, W. Xiang, J. Xie, J.H. He, R.K. Kotlanka, S.P. Low, H. Feng, Electromagnetic energy harvesting from vibrations of multiple frequencies, *Journal of micromechanics and microengineering* 19(3) (2009) 035001.
- [14] A.K. Batra, A. Alomari, *Power harvesting via smart materials*, SPIE Press Bellingham, WA2017.

- [15] Y. Zhang, T. Wang, A. Luo, Y. Hu, X. Li, F. Wang, Micro electrostatic energy harvester with both broad bandwidth and high normalized power density, *Applied energy* 212 (2018) 362-371.
- [16] F. Orfei, Introduction to Vibration Energy Harvesting, August 19, 2019. <https://www.allaboutcircuits.com/technical-articles/introduction-to-vibration-energy-harvesting/>. (Accessed 31.01.2023).
- [17] D. Fourie, Shoe-mounted PVDF piezoelectric transducer for energy harvesting, *MORJ rev.* 19 (2010) 66-70.
- [18] H. Kim, V. Bedekar, R.A. Islam, W.-H. Lee, D. Leo, S. Priya, Laser-machined piezoelectric cantilevers for mechanical energy harvesting, *IEEE transactions on ultrasonics, ferroelectrics, and frequency control* 55(9) (2008) 1900-1905.
- [19] S.M. Kargar, G. Hao, An Atlas of Piezoelectric Energy Harvesters in Oceanic Applications, *Sensors* 22(5) (2022) 1949.
- [20] W. Heywang, K. Lubitz, W. Wersing, Piezoelectricity: evolution and future of a technology, Springer Science & Business Media 2008.
- [21] H. Li, C. Tian, Z.D. Deng, Energy harvesting from low frequency applications using piezoelectric materials, *Applied physics reviews* 1(4) (2014) 041301.
- [22] S. Roundy, P.K. Wright, A piezoelectric vibration based generator for wireless electronics, *Smart Materials and structures* 13(5) (2004) 1131.
- [23] S. Li, A. Crovetto, Z. Peng, A. Zhang, O. Hansen, M. Wang, X. Li, F. Wang, Bi-resonant structure with piezoelectric PVDF films for energy harvesting from random vibration sources at low frequency, *Sensors and Actuators A: Physical* 247 (2016) 547-554.
- [24] C.V. Karadag, N. Topaloglu, A self-sufficient and frequency tunable piezoelectric vibration energy harvester, *Journal of Vibration and Acoustics* 139(1) (2017).
- [25] G. Acciani, F. Di Modugno, G. Gelao, E. Mininno, Shape optimization of cantilever beam for wind energy harvesting, 2015 International Conference on Renewable Energy Research and Applications (ICRERA), IEEE, 2015, pp. 1207-1212.
- [26] X. Shan, H. Tian, D. Chen, T. Xie, A curved panel energy harvester for aeroelastic vibration, *Applied Energy* 249 (2019) 58-66.
- [27] Z. Yang, Y.Q. Wang, L. Zuo, J. Zu, Introducing arc-shaped piezoelectric elements into energy harvesters, *Energy conversion and management* 148 (2017) 260-266.
- [28] L. Zuo, X. Tang, Large-scale vibration energy harvesting, *Journal of intelligent material systems and structures* 24(11) (2013) 1405-1430.

[29] H.S. Kim, J.-H. Kim, J. Kim, A review of piezoelectric energy harvesting based on vibration, *International journal of precision engineering and manufacturing* 12(6) (2011) 1129-1141.

[30] K.-c. Chuang, H.-s. Tzou, PVDF energy harvester on flexible rings, *Proceedings of the 2010 Symposium on Piezoelectricity, Acoustic Waves and Device Applications*, IEEE, 2010, pp. 100-105.

[31] Z.-Q. Lu, D. Wu, H. Ding, L.-Q. Chen, Vibration isolation and energy harvesting integrated in a Stewart platform with high static and low dynamic stiffness, *Applied Mathematical Modelling* 89 (2021) 249-267.

[32] Z.-Q. Lu, D. Shao, Z.-W. Fang, H. Ding, L.-Q. Chen, Integrated vibration isolation and energy harvesting via a bistable piezo-composite plate, *Journal of Vibration and Control* 26(9-10) (2020) 779-789.

